CONVERGENT FINITE ELEMENT METHODS FOR THE PERFECT CONDUCTIVITY PROBLEM WITH CLOSE-TO-TOUCHING INCLUSIONS

BUYANG LI, HAIGANG LI, AND ZONGZE YANG

Abstract. In the perfect conductivity problem (i.e., the conductivity problem with perfectly conducting inclusions), the gradient of the electric field is often very large in a narrow region between two inclusions and blows up as the distance between the inclusions tends to zero. The rigorous error analysis for the computation of such perfect conductivity problems with close-to-touching inclusions of general geometry still remains open in three dimensions. We address this problem by establishing new asymptotic estimates for the second-order partial derivatives of the solution with explicit dependence on the distance ε between the inclusions, and use the asymptotic estimates to design a class of graded meshes and finite element spaces to solve the perfect conductivity problem with possibly close-to-touching inclusions. In particular, we propose a special finite element basis function which resolves the asymptotic singularity of the solution by making the interpolation error bounded in $W^{1,\infty}$ in a neighborhood of the close-to-touching point, even though the solution itself is blowing up in $W^{1,\infty}$. This is crucial in the error analysis for the numerical approximations. We prove that the proposed method yields optimal-order convergence in the H^1 norm, uniformly with respect to the distance ε between the inclusions, in both two and three dimensions for general convex smooth inclusions which are possibly close-to-touching. Numerical experiments are presented to support the theoretical analysis and to illustrate the convergence of the proposed method for different shapes of inclusions in both two- and three-dimensional domains.

1. Introduction

This article is concerned with the problem of electric conduction in high-contrast fiber-reinforced composite materials with embedded inclusions which may be close together and almost touching. As the inclusions approach closely, the gradient of the solution of this problem tends to blow-up in the narrow region between the inclusions, which brings many challenges to the numerical computation.

To illustrate this problem in a simple setting, we consider a bounded domain $D \subset \mathbb{R}^n$, $n \in \{2,3\}$, which contains two convex smooth inclusions $D_1 \subset D$ and $D_2 \subset D$ such that the distance $\varepsilon = \mathrm{dist}(D_1, D_2)$ is possibly very small and D_1 and D_2 are far away from the piecewise smooth boundary $\Gamma := \partial D$, as shown in Figure 1.1. We assume the $C^{2,\alpha}$-norm of ∂D_1 and ∂D_2 are bounded, and the curvature of ∂D_1 and ∂D_2 are bounded from below. The voltage potential u in the conductivity problem with a given boundary value $\varphi \in H^{\frac{3}{2}}(\Gamma)$ can be described by the partial differential equation (PDE)

$$\begin{cases} \nabla \cdot (a(x)\nabla u) = 0 & \text{in } D, \\ u = \varphi & \text{on } \Gamma, \end{cases} \tag{1.1}$$

2010 *Mathematics Subject Classification.* 65M12, 65M15, 76D05.

Key words and phrases. Perfect conductivity problem, composite materials, asymptotic estimates, singularity, finite element method, graded mesh, error estimates.

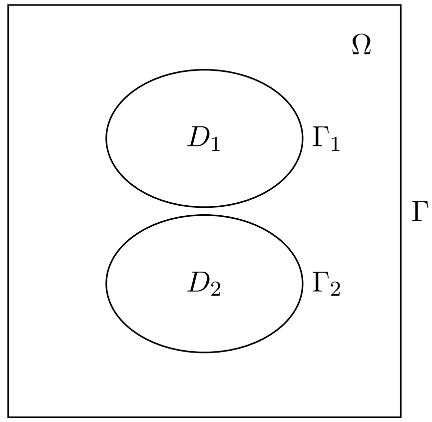

FIGURE 1.1. The domain $\Omega = D\backslash\overline{D_1 \cup D_2}$.

where $H^{\frac{3}{2}}(\Gamma) := \{v|_\Gamma : v \in H^2(D)\}$ and $a(x)$ is a piecewise constant function defined by

$$a(x) = \begin{cases} k & \text{for } x \in D_1 \cup D_2, \\ 1 & \text{for } x \in D\backslash\overline{D_1 \cup D_2}, \end{cases}$$

which represents the (renormalized) conductivity in the two different materials. Without loss of generality, the boundary value $\varphi \in H^{\frac{3}{2}}(\Gamma)$ can be extended to $\varphi \in H^2(D)$ such that $\varphi = 0$ in a neighborhood of the convex envelope of $\overline{D_1 \cup D_2}$. Then equation (1.1) is equivalent to finding the minimizer $u \in \varphi + H_0^1(D)$ of the energy functional

$$E_k[u] := \frac{k}{2}\int_{D_1 \cup D_2} |\nabla u|^2 + \frac{1}{2}\int_{D\backslash\overline{D_1 \cup D_2}} |\nabla u|^2.$$

When k is away from 0 and ∞, the gradient of the solution to the conductivity problem (1.1) is bounded uniformly with respect to the distance ε. This has been proved in [3, 9, 16, 36] under different conditions. However, when $k = \infty$ in (1.1), the situation is quite different. The L^∞-norm of the electric field ∇u is often very large in the narrow region between the two inclusions and blows up as $\varepsilon = \operatorname{dist}(D_1, D_2) \to 0$. The analysis and computation of such asymptotic behaviour of the electric field has attracted much attention from physicists and applied/computational mathematicians; see [1, 2, 6, 8, 15, 24, 26, 27, 36, 39–42] and the references therein.

The limiting case $k \to \infty$ of this problem corresponds to the conductivity problem with perfectly conducting inclusions (called the perfect conductivity problem), which characterizes the asymptotic behaviour with respect to ε. By denoting $\Omega = D\backslash\overline{D_1 \cup D_2}$ and $\Gamma_j = \partial D_j$, $j = 1, 2$, the perfect conductivity problem with boundary value φ can be described as finding the minimizer $u \in \varphi + \mathring{H}_c^1(\Omega)$ of the following energy functional

$$E_\infty[u] := \frac{1}{2}\int_\Omega |\nabla u|^2,$$

where

$$\mathring{H}_c^1(\Omega) = \left\{v \in H_c^1(\Omega) : v = 0 \text{ on } \Gamma\right\}$$

with $H_c^1(\Omega) = \{v \in H^1(\Omega) : \exists\, c_1, c_2 \in \mathbb{R} \text{ with } v|_{\Gamma_i} = c_i \text{ for } i = 1,2\}$. This is equivalent to the following PDE boundary value problem:

$$\begin{cases} \Delta u = 0 & \text{in } \Omega, \\ u = c_j & \text{on } \Gamma_j, j = 1,2, \\ \int_{\Gamma_j} \partial_n u = 0 & j = 1,2, \\ u = \varphi & \text{on } \Gamma, \end{cases} \tag{1.2}$$

where c_1 and c_2 are free constants to be determined by the conditions $\int_{\Gamma_1} \partial_n u = \int_{\Gamma_2} \partial_n u = 0$.

For the perfect conductivity problems in (1.2), the gradient of the electric field is very large in the narrow region between the two inclusions, and blows up as $\varepsilon = \operatorname{dist}(D_1, D_2)$ tends to zero. The asymptotic estimates for the gradient of the solution to the perfect conductivity problem have been established for circular inclusions in [24,25,33] and for general convex smooth inclusions [30, 32]. In particular, by denoting $x' = (x_1, \cdots, x_{n-1})$, if the boundaries of the two convex smooth inclusions can be described (locally in a neighborhood of the origin) by the following two graphs:

$$\partial D_j \cap \left\{x : |x'| \le \frac{1}{2}\right\} = \{x \in \mathbb{R}^n : x_n = \phi_j(x')\}, \;\; j = 1,2, \;\text{ for } |x'| \le \frac{1}{2}, \tag{1.3}$$

with

$$\phi_1(0) = -\phi_2(0) = \frac{\varepsilon}{2}, \quad \nabla\phi_1(0) = \nabla\phi_2(0) = 0 \quad \text{and} \quad \rho\big(\nabla^2(\phi_1 - \phi_2)(0)\big) \ge \lambda_0,$$

where $\rho(A)$ denotes the smallest eigenvalue of a matrix A and λ_0 is some fixed positive constant, then the following asymptotic estimates have been proved for $x = (x', x_n) \in \Omega$ such that $|x'| \le \frac{1}{2}$:

$$|\nabla u| \lesssim \begin{cases} \dfrac{\sqrt{\varepsilon}}{\varepsilon + |x_1|^2} + O(1) & \text{for } n = 2, \\[2ex] \dfrac{1}{|\log\varepsilon|(\varepsilon + |x_1|^2 + |x_2|^2)} + O(1) & \text{for } n = 3. \end{cases} \tag{1.4}$$

As the distance $\varepsilon = \operatorname{dist}(D_1, D_2)$ between the two inclusions tends to zero, the gradient of the solution in three dimensions is asymptotically $O(\varepsilon^{-1}/|\log\varepsilon|)$ on the segment

$$L_\varepsilon = \left\{x \in \mathbb{R}^n : |x'| = 0, \; |x_n| \le \frac{\varepsilon}{2}\right\}.$$

Such asymptotic singularities make the numerical computation of these problems challenging. Here we would like to mention that the insulated conductivity problem for $k = 0$ is also an interesting problem, see [17, 37, 47] for example.

Some integral equation methods and expansion methods have been shown successful in approximating the solution of such conductivity problems in composite materials under different situations, including the fast-multipole integral equation methods [20], the fast-multipole iterative schemes [21, 22], the method of images [12, 13], and a hybrid basis scheme [14] which addresses the challenge of close-to-touching inclusions for discs inclusions in two dimensions. These methods mainly focus on the conductivity problem on the two-dimensional plane, with mildly close inclusions of general geometry or close-to-touching discs inclusions. A spectral Galerkin approximation of an integral equation formulation was proposed in [38] for spherical inclusions in three dimensions. The method has spectral convergence for smooth solutions, while the error analysis for close-to-touching inclusions (when the solution is asymptotically singular) still remains open. In [24] the authors characterized explicitly the singular term of the solution for two circular inclusions and showed that the characterization of the singular term can be used efficiently for computation of the gradient in the presence close-to-touching inclusions based on the boundary integral method. The result could also be extended to perfect conductors of spherical shape in three dimensions. Rigorous error estimates of the integral equation methods for the asymptotical singular solutions of the perfect conductivity problem, with close-to-touching inclusions of general geometry, still remain open in three dimensions.

The finite element methods are convenient for solving the perfect conductivity problem in bounded domains with inclusions of general geometry. However, the existing finite element error analyses do not address the perfect conductivity problem with close-to-touching inclusions. The finite element methods for the conductivity problem with bounded k and large gap between the inclusions, using flat segments/faces to approximate the curved interfaces, have been well studied in the literature. In particular, optimal-order L^2 and H^1 error estimates for the corresponding elliptic interface problems were established in [5, 11, 23, 45, 46]. The error estimates of higher-order finite element methods with isoparametric finite elements for approximating the smooth interfaces were presented in [35]. There are still no rigorous error estimates of any finite element methods uniform with respect to $\varepsilon = \mathrm{dist}(D_1, D_2)$ for such perfect conductivity problems in composite materials with possibly close-to-touching inclusions. The development of finite element methods and corresponding error analysis for such problems rely on the asymptotic estimates of higher-order partial derivatives of the solution, which also have not been established.

In this article, we develop new asymptotic estimates and finite element methods, with rigorous proof of convergence of the finite element solutions, for the perfect conductivity problem in (1.2), with possibly close-to-touching perfectly conducting inclusions as shown in Figure 1.1. Namely, (1.2) is the problem of interest that we consider in this article, while (1.1) is just for introduction to the conductivity problem in a general context. The main contribution of this article includes the following several aspects:

- Pointwise asymptotic estimates for the second-order partial derivatives of the solution are established for the first time. This shows the specific asymptotic behaviour (blow-up rate) of the second-order partial derivatives as $\varepsilon \to 0$.
- Based on the pointwise asymptotic estimates, we propose a new class of graded meshes and finite element spaces, with a new finite element basis adapted to the asymptotic behaviour of the solution in the close-to-touching case, in order to resolve the asymptotic singularity of the solution at the segment L_ε. In particular, we propose a special finite element basis function in a neighborhood of the close-to-touching point (see Section 2.2, Case 2). This special finite element basis function resolves the asymptotic singularity of the gradient by making the interpolation error of the solution bounded in $W^{1,\infty}$ in a neighborhood of the close-to-touching point, even though the solution itself is blowing up in $W^{1,\infty}$; see Lemma 3.1. This is crucial in the error analysis for the numerical approximations.
- Rigorous error estimates are established for the finite element solutions with optimal-order convergence in the H^1 norm uniform with respect to the distance $\varepsilon = \mathrm{dist}(D_1, D_2)$ between the inclusions. Both the computational cost and convergence rate are independent of $\varepsilon = \mathrm{dist}(D_1, D_2)$ and therefore can be applied to the case with close-to-touching inclusions.
- Both two- and three-dimensional problems with possibly close-to-touching inclusions are covered in a unified framework. The results hold for the perfect conductivity problem in a bounded domain with general convex smooth inclusions (not only restricted to circles or spheres).
- The methodology proposed in this article for obtaining the asymptotic estimates, the graded mesh and the finite element spaces, and the error estimates, may also be extended

to other related problems with possibly close-to-touching inclusions, such as the stress concentration problem in high-contrast elastic composite materials.

- Benchmark examples with spherical and ellipsoidal close-to-touching inclusions are presented in both two- and three-dimensions.

For the simplicity of notation, we denote by C a generic positive constant which may be different at each occurrence but is always independent of the distance parameter ε and the mesh size h of the finite element method. We also denote by $A \lesssim B$ the statement "$A \leq CB$ for some constant C", and denote by $A \sim B$ the statement "$C^{-1}B \leq A \leq CB$ for some constant C".

2. Main results

In this section, we present the main theoretical results of this article, including the asymptotic estimates for the second-order partial derivatives of the solution, the design of graded meshes and finite element spaces for approximating the solution, and the error estimates for the finite element method.

2.1. Estimates for the second-order partial derivatives

We prove the following asymptotic estimates for the second-order partial derivatives of the solution to the perfect conductivity problem.

Theorem 2.1. *Suppose that D is a bounded convex domain with piecewise smooth boundary Γ, and $\varphi \in H^{\frac{3}{2}}(\Gamma)$, while D_1 and D_2 are convex and smooth. Moreover, the boundaries of the two inclusions in the region $\{x \in \mathbb{R}^n : |x'| \leq \frac{1}{2}, |x_n| \leq \frac{1}{2}\}$ can be described by the two graphs in* (1.3)*. Then the solution of* (1.2) *satisfies the following estimates for $x = (x', x_n) \in \Omega$ such that $|x'| \leq \frac{1}{2}$:*

$$|\nabla^2 u| \lesssim \frac{1}{\varepsilon + |x'|^2} \ \textit{for } n = 2, \quad \textit{and} \quad |\nabla^2 u| \lesssim \frac{1}{|\log \varepsilon|(\varepsilon + |x'|^2)^{\frac{3}{2}}} \ \textit{for } n = 3.$$

This kind of estimates for the second-order partial derivatives obtained in Theorem 2.1 is new, which is crucial for us to design a class of graded meshes and finite element spaces to approximate the solution by resolving the asymptotic singularity at the segment L_ε.

2.2. The design of graded mesh and finite element space

In order to obtain optimal-order convergence of the finite element solutions by resolving the asymptotic singularity of the solution as $\varepsilon \to 0$, we divide the domain Ω into the following dyadic subregions (Figure 2.1)

$$\Omega_j = \big\{x \in \Omega : \phi_1(x') \leq x_n \leq \phi_2(x'),\ \ 2^{-j-1} \leq |x'| < 2^{-j}\big\}, \tag{2.1}$$

$$\Omega_* = \big\{x \in \Omega : \phi_1(x') \leq x_n \leq \phi_2(x'),\ \ |x'| < 2^{-J-1}\big\}, \tag{2.2}$$

$$\Omega_*^c = \Omega \backslash \overline{\Omega}_*, \tag{2.3}$$

$$\Omega_0 = \Omega \backslash \big(\Omega_* \cup \cup_{j=1}^{J} \Omega_j\big), \tag{2.4}$$

and design a class of graded meshes of maximal mesh size $h > 0$ subject to the partition of the domain in (2.1)–(2.4).

We consider the following two cases separately. Case 1: For a given maximal mesh size h, the elements generated by a graded mesh are small enough to fill in the close-to-touching zone. Case 2: The elements are not small enough to fill in the close-to-touching zone, and we construct a

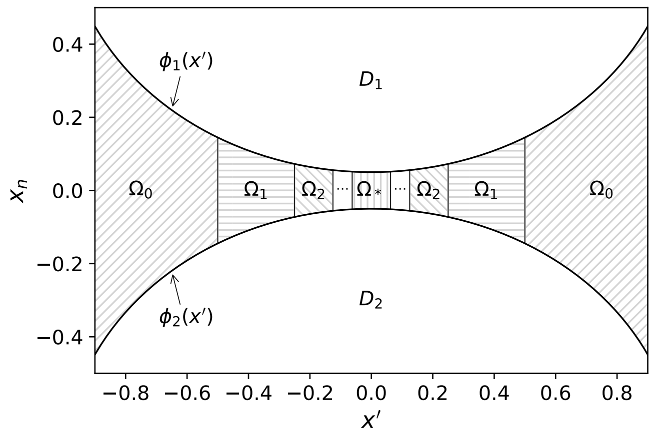

FIGURE 2.1. Illustration of the dyadic subregions Ω_j and Ω_*.

special element for the close-to-touching zone. Accordingly, the graded meshes will be generated based on the two parameters: A parameter $\kappa \geq 1$ which helps us to divide the problem into the above-mentioned two cases, and a parameter $\alpha \in (\frac{n-1}{2}, 1+\frac{1}{n})$ which represents the rate of mesh refinement towards the segment L_ε, i.e., the local mesh size $h(x) = O(h|x'|^\alpha)$ is chosen, where the lower bound of α guaranties the resolution of the singularity and the upper bound of α guaranties that the number of elements is $O(h^{-n})$ (so the computational cost is equivalent to using quasi-uniform triangulation of mesh size h). Both parameters κ and α should be chosen a priori and fixed, independent of ε and h. Then the mesh could be generated by considering the following two different cases (for various different values of ε and h):

(1) Case 1: $\varepsilon \geq (\kappa h)^{\frac{1}{1-\alpha/2}}$. In this case, for the given ε and h, we choose J to satisfy $2^{-J} \sim \varepsilon^{\frac{1}{2}}$ and consider a locally quasi-uniform triangulation of the domain Ω in such a way that the diameters of the triangles/tetrahedra in each Ω_0, Ω_j and Ω_* are equivalent, denoted by h, h_j and h_*, respectively, satisfying the following conditions:

$$h_j \sim |x'|^\alpha h \sim 2^{-\alpha j} h \quad \text{and} \quad h_* \sim 2^{-\alpha J} h.$$

Moreover, the triangulation approximates the smooth boundary Γ and Γ_j, $j = 1, 2$, with piecewise flat lines (in 2D) or triangles (in 3D).

(i) We denote by $\mathcal{K}_h$ the set of closed triangles/tetrahedra in the triangulation of Ω, and denote by $\Omega_h = \left(\bigcup_{K\in\mathcal{K}_h} K\right)^\circ$ the corresponding open polygonal/polyhedral approximation of Ω, where B° denotes the interior of a set $B \subset \mathbb{R}^n$. Let Γ_h, $\Gamma_{1,h}$ and $\Gamma_{2,h}$ be the corresponding polygonal/polyhedral approximations of Γ, Γ_1 and Γ_2, respectively.

(ii) The condition $\varepsilon \geq (\kappa h)^{\frac{1}{1-\alpha/2}}$ guarantees that $|x'|^\alpha h \leq \kappa^{-1}|x'|^2$ for $|x'| \geq \varepsilon^{\frac{1}{2}}$. This means that $h_j \leq \kappa^{-1}(\varepsilon + |x'|^2)$ for $x \in \Omega_j$ so that the region between $\Gamma_{1,h}$ and $\Gamma_{2,h}$ can be filled in with triangles (by choosing a sufficiently large fixed constant κ which is independent of ε and h).

(iii) For $|x'| \leq \varepsilon^{\frac{1}{2}}$ the diameters of the triangles/tetrahedra are equivalent to h_*, which satisfies $h_* \sim \varepsilon^{\frac{\alpha}{2}} h \leq \kappa^{-1}\varepsilon$ as a result of $\varepsilon \geq (\kappa h)^{\frac{1}{1-\alpha/2}}$. Therefore, by choosing a sufficiently large constant κ (independent of ε and h), the region between $\Gamma_{1,h}$ and $\Gamma_{2,h}$ can be filled in with triangles/tetrahedra.

(iv) We define the following finite element spaces:

$$S_h(\Omega_h) = \{v \in H^1(\Omega_h) : v|_K \in \mathbb{P}_1(K)\},$$
$$S_{h,c}(\Omega_h) = \{v \in S_h(\Omega_h) : v = \text{constants on } \Gamma_{1,h} \text{ and } \Gamma_{2,h}\},$$
$$\mathring{S}_{h,c}(\Omega_h) = \{v \in S_{h,c}(\Omega_h) : v = 0 \text{ on } \Gamma_h\}.$$

Hence, the finite element space is conforming in Case 1.

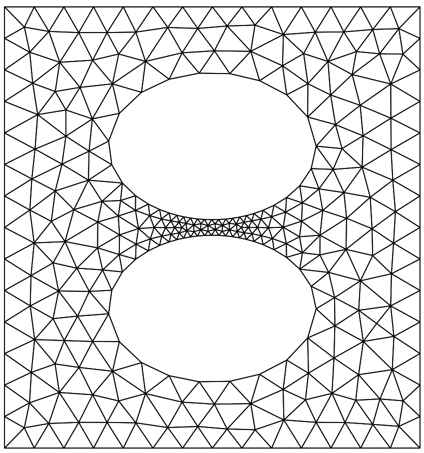

(a) Mesh in Case 1

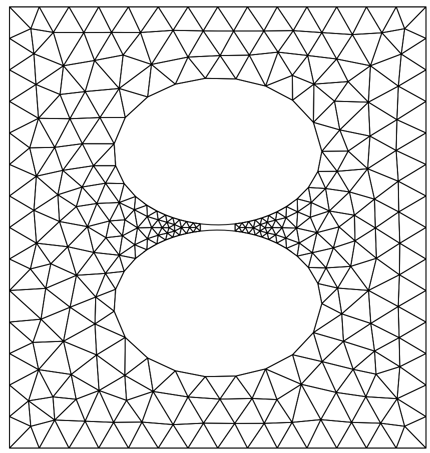

(b) Mesh in Case 2

FIGURE 2.2. Graded mesh in the two cases $\varepsilon \geq (\kappa h)^{\frac{1}{1-\alpha/2}}$ and $\varepsilon \leq (\kappa h)^{\frac{1}{1-\alpha/2}}$

Remark 2.1. *The conditions $h_j \sim |x'|^\alpha h \sim 2^{-\alpha j}h$ and $h_* \sim 2^{-\alpha J}h$ for the mesh sizes could be satisfied by choosing, for example,*

$$\frac{1}{20}|x'|^\alpha h \leq h_j \leq \frac{1}{5}|x'|^\alpha h \quad \text{and} \quad \frac{1}{20}2^{-\alpha J}h \leq h_* \leq \frac{1}{5}2^{-\alpha J}h.$$

Then $h_j \leq \frac{1}{5}\kappa^{-1}(\varepsilon + |x'|^2)$ for $x \in \Omega_j$ in the case $\varepsilon \geq (\kappa h)^{\frac{1}{1-\alpha/2}}$, which guarantees that $|x'|^\alpha h \leq \kappa^{-1}|x'|^2$ for $|x'| \geq \varepsilon^{\frac{1}{2}}$. In addition, we could choose J sufficiently large so that $\frac{1}{2}\varepsilon^{\frac{1}{2}} \leq 2^{-J} \leq \varepsilon^{\frac{1}{2}}$. Then $h_* \leq \frac{1}{5}2^{-\alpha J}h \leq \frac{1}{5}\varepsilon^{\frac{\alpha}{2}}h$. Thus the conditions $h_j \leq \frac{1}{5}\kappa^{-1}(\varepsilon + |x'|^2)$ for $x \in \Omega_j$ and $h_* \leq \frac{1}{5}\kappa^{-1}\varepsilon$ for $|x'| \leq \varepsilon^{\frac{1}{2}}$ are both satisfied. The choice of the constants $\frac{1}{20}$ and $\frac{1}{5}$ in determining the mesh sizes h_j and h_* are not unique and could be adjusted in practical computation.

(2) Case 2: $\varepsilon \leq (\kappa h)^{\frac{1}{1-\alpha/2}}$. In this case, we choose J to satisfy $2^{-J-1} \sim (\kappa h)^{\frac{1}{2-\alpha}}$ so that

$$\Omega_* = \{x \in \Omega : |x'| < 2^{-J-1} \sim (\kappa h)^{\frac{1}{2-\alpha}}\}.$$

Let $\Omega_*^c = \Omega \backslash \overline{\Omega}_*$ and denote by $\Gamma_* = \partial\Omega_*^c \cap \partial\Omega_*$ the interface between the two subregions Ω_*^c and Ω_*. We triangulate the subregion Ω_*^c with the triangulation fitting the edges (or points in two dimensions) at $\partial D_j \cap \Gamma_*$, $j = 1, 2$, and denote the triangulated approximate domain by $\Omega_{*,h}^c$. The region Ω_* is not triangulated.

In the region Ω_*^c it holds that $|x'|^\alpha h \le \kappa^{-1}|x'|^2$ and therefore $h_j \lesssim \kappa^{-1}|x'|^2$. On the interface $\Gamma_* = \partial\Omega_*^c \cap \partial\Omega_*$ it holds that $|x'|^\alpha h \sim \kappa^{-1}|x'|^2$ with $|x'| \sim 2^{-J}$, and therefore

$$h_* \sim 2^{-\alpha J} h \sim |x'|^\alpha h \sim \kappa^{-1}|x'|^2 \sim \kappa^{-1}(\varepsilon + |x'|^2) \quad \text{for } x \in \Gamma_*. \tag{2.5}$$

(i) We denote by $\mathcal{K}_h$ the set of triangles/tetrahedra in $\Omega_{*,h}^c$. Let Γ_h, $\Gamma_{1,h}$ and $\Gamma_{2,h}$ be the corresponding approximations of Γ, Γ_1 and Γ_2, respectively, where $\Gamma_{1,h}$ and $\Gamma_{2,h}$ are curved in the region $|x'| \le (\kappa h)^{\frac{1}{2-\alpha}}$. Namely, $\Gamma_{1,h} = \Gamma_1$ and $\Gamma_{2,h} = \Gamma_2$ in the region corresponding to $|x'| \le (\kappa h)^{\frac{1}{2-\alpha}}$.

(ii) In the region Ω_*^c it holds that $|x'| \gtrsim (\kappa h)^{\frac{1}{2-\alpha}}$, which guarantees

$$h_j \le \kappa^{-1}|x'|^2 \le \kappa^{-1}(\varepsilon + |x'|^2)$$

for $x \in \Omega_j$ so that (for sufficiently large $\kappa \ge 1$ that is independent of ε) the region between $\Gamma_{1,h}$ and $\Gamma_{2,h}$ can be filled in with triangles.

(iii) We define the following finite element spaces on $\Omega_{*,h}^c$:

$$S_h(\Omega_{*,h}^c) = \{v_h \in H^1(\Omega_{*,h}^c) : v_h|_K \in \mathbb{P}_1(K) \text{ for every tetrahedron } K \subset \Omega_{*,h}^c\}$$

and define $S_{h,c}(\Omega_{*,h}^c)$ as the subspace of $S_h(\Omega_{*,h}^c)$ consisting of functions v_h which are constants on $\Gamma_{j,h}$ and

$$v_h(x', x_n) = v_h|_{\Gamma_{1,h}} \frac{x_n - \phi_2(x')}{\phi_1(x') - \phi_2(x')} + v_h|_{\Gamma_{2,h}} \frac{\phi_1(x') - x_n}{\phi_1(x') - \phi_2(x')} \quad \text{at the nodes on } \Gamma_*.$$

Let $\mathring{S}_{h,c}(\Omega_{*,h}^c) = \{v \in S_{h,c}(\Omega_{*,h}^c) : v = 0 \text{ on } \Gamma_h\}$. For any $v_h \in S_{h,c}(\Omega_{*,h}^c)$ we define $v_h^* \in H^1(\Omega_*)$ as

$$v_h^*(x', x_n) = v_h|_{\Gamma_{1,h}} \frac{x_n - \phi_2(x')}{\phi_1(x') - \phi_2(x')} + v_h|_{\Gamma_{2,h}} \frac{\phi_1(x') - x_n}{\phi_1(x') - \phi_2(x')} \quad \text{for } x \in \Omega_*. \tag{2.6}$$

In particular, a finite element function $v_h \in S_{h,c}(\Omega_{*,h}^c)$ is piecewise linear on $\Omega_{*,h}^c$ and matches the values of v_h^* at the nodes on the interface Γ_*.

An example of graded mesh in the two cases $\varepsilon \ge (\kappa h)^{\frac{1}{1-\alpha/2}}$ and $\varepsilon \le (\kappa h)^{\frac{1}{1-\alpha/2}}$ is presented in Figure 2.2. The role of the graded mesh defined above will become clear in the error estimation for the finite element method. In particular, in the second case $\varepsilon \le (\kappa h)^{\frac{1}{1-\alpha/2}}$, the modification of the finite element space in the region Ω_* is of essential help to obtain an error estimate independent of ε.

Remark 2.2. The expression in (2.6) can be written as

$$v_h(x', x_n) = (b_1 - b_2)\bar{v}_1 + b_2 \quad \text{with } \bar{v}_1(x', x_n) = \frac{x_n - \phi_2(x')}{\phi_1(x') - \phi_2(x')}.$$

In Section 4, inequalities (4.15) and (4.16), we will see that the solution u of (1.2) has the following decomposition:

$$\nabla u = \nabla[(c_1 - c_2)\bar{v}_1 + c_2] + \nabla R \quad \text{in } \Omega_*,$$

with c_1 and c_2 being the constant values of u on Γ_1 and Γ_2, respectively, and R is a function satisfying the following estimate:

$$\|\nabla R\|_{L^\infty(\Omega_*)} \lesssim 1.$$

This is why we add a basis function in the form of (2.6) to the finite element space, as it resolves the asymptotic singularity of the solution. Namely, finite element functions in the form of $(b_1 - b_2)\bar{v}_1 + b_2$, with $b_1, b_2 \in \mathbb{R}$, could approximate u with a remainder uniformly bounded with respect to ε in $W^{1,\infty}(\Omega_*)$, while the solution u itself is not uniformly bounded with respect to ε in $W^{1,\infty}(\Omega_*)$ in view of the estimate in (1.4).

In Section 4, inequalities (4.3) and (4.6), we will see that for $\delta(x') \sim \varepsilon + |x'|^2$ the following estimate holds:

$$
\begin{aligned}
|\nabla^2[(c_1 - c_2)\bar{v}_1 + c_2]| &\lesssim |c_1 - c_2| \Big(\frac{1}{\delta(x')^2} + \frac{|x'|}{\delta(x')^2} \Big) \\
&\lesssim \begin{cases} \dfrac{1}{\varepsilon + |x'|^2} & \text{for } \ n = 2 \\[2ex] \dfrac{1}{|\log \varepsilon| (\varepsilon + |x'|^2)^{\frac{3}{2}}} & \text{for } \ n = 3. \end{cases}
\end{aligned}
$$

Thus the singular behaviour of $\nabla^2[(c_1 - c_2)\bar{v}_1 + c_2]$ is the same as that of $\nabla^2 u$ in Theorem 2.1.

Remark 2.3. In both Case 1 and Case 2, the following inequality holds when h is sufficiently small (smaller than some constant which is independent of ε):

$$
h_j \le \frac{2^{-j}}{10}, \tag{2.7}
$$

which implies that the set of triangles/tetrahedra which intersect Ω_j is contained in $\Omega_j' := \Omega_{j-1} \cup \Omega_j \cup \Omega_{j+1}$. Relation (2.7) is equivalent to $2^{-\alpha j} h \lesssim \frac{2^{-j}}{10}$, which can be satisfied if

$$
h \lesssim o(1) 2^{-(1-\alpha)J}.
$$

where $o(1)$ denotes a quantity which tends to zero as $h \to 0$. Since $h \lesssim o(1)(\kappa h)^{\frac{1-\alpha}{2-\alpha}}$, it suffices to prove that

$$
(\kappa h)^{\frac{1-\alpha}{2-\alpha}} \lesssim 2^{-(1-\alpha)J}. \tag{2.8}
$$

In Case 1, we have $2^{-J} \sim \varepsilon^{\frac{1}{2}}$ and $\varepsilon \ge (\kappa h)^{\frac{1}{1-\alpha/2}}$, which imply (2.8). In Case 2, we have $2^{-J-1} \sim (\kappa h)^{\frac{1}{2-\alpha}}$, which also implies (2.8). This proves that (2.7) holds when h is sufficiently small (smaller than some constant which is independent of ε).

2.3. The interpolation operator and its local error estimates

In Case 1, $\varepsilon \ge (\kappa h)^{\frac{1}{1-\alpha/2}}$, the whole domain Ω is triangulated to Ω_h, and we denote by $I_h : C(\overline{\Omega}) \cap H^1_c(\Omega) \to S_{h,c}(\Omega_h)$ the standard Lagrange interpolation operator such that

$$
I_h v = v \quad \text{at all finite element nodes of } \Omega_h, \ \forall\, v \in C(\overline{\Omega}).
$$

This standard Lagrange interpolation operator satisfies the following standard estimates:

$$
\|v - I_h v\|_{L^\infty(\Omega_j)} \lesssim \|v\|_{W^{k,\infty}(\Omega_j)} h_j^k \quad \text{for } \ k = 1, 2.
$$

In Case 2, $\varepsilon \le (\kappa h)^{\frac{1}{1-\alpha/2}}$, only the subdomain Ω_*^c is triangulated to $\Omega_{*,h}^c$. For $v \in H^1_c(\Omega) \cap C(\overline{\Omega})$, we define

$$
(I_h^* v)(x', x_n) = v|_{\Gamma_1} \frac{x_n - \phi_2(x')}{\phi_1(x') - \phi_2(x')} + v|_{\Gamma_2} \frac{\phi_1(x') - x_n}{\phi_1(x') - \phi_2(x')} \quad \text{for } \ x \in \Omega_*, \tag{2.9}
$$

and define $I_h v \in S_h(\Omega_{*,h}^c)$ by requiring $I_h v = v$ at all finite element nodes of $\Omega_{*,h}^c \backslash \Gamma_*$ and $I_h v = I_h^* v$ at the finite element nodes of Γ_* (thus $I_h v$ and $I_h^* v$ match each other at the nodes on the interface Γ_*). This defines a Lagrange interpolation operator $I_h : H^1_c(\Omega) \cap C(\overline{\Omega}) \to S_{h,c}(\Omega_{*,h}^c)$.

This interpolation can also be restricted to the subspace with zero boundary condition on Γ, i.e., $I_h : \mathring{H}^1_c(\Omega) \cap C(\overline{\Omega}) \to \mathring{S}_{h,c}(\Omega^c_{*,h})$.

2.4. The deformed finite element space and interpolation operator

In Case 1, $\varepsilon \geq (\kappa h)^{\frac{1}{1-\alpha/2}}$, the whole domain Ω is triangulated and there exists a one-to-one Lipschitz continuous map $\Phi_h : \Omega_h \to \Omega$ such that

$$\|\Phi_h - \mathrm{id}\|_{L^\infty(\Omega_h)} \lesssim h^2, \quad \|\nabla\Phi_h - I\|_{L^\infty(\Omega_h)} \lesssim h, \tag{2.10}$$

where id denotes the identity function such that $\mathrm{id}(x) = x$ for all $x \in \mathbb{R}^d$, and $I = \nabla\mathrm{id}$ denotes the $d \times d$ identity matrix; see [28] for the existence of the map $\Phi_h : \Omega_h \to \Omega$ satisfying the estimate in (2.10). In particular, since the error $\Phi_h - \mathrm{id}$ is only from approximating the curved boundary by flat lines (in 2D) or flat triangles (in 3D), it only depends on h and is independent of ε. For a finite element function $v_h \in \mathring{S}_{h,c}(\Omega_h)$, we define $v_h^* := v_h \circ \Phi_h^{-1}$ on Ω.

In Case 2, $\varepsilon \leq (\kappa h)^{\frac{1}{1-\alpha/2}}$, only the subdomain Ω^c_* is triangulated, and there exists a one-to-one Lipschitz continuous map $\Phi_h : \Omega^c_{*,h} \to \Omega^c_*$ such that

$$\|\Phi_h - \mathrm{id}\|_{L^\infty(\Omega^c_{*,h})^n} \lesssim h^2, \quad \|\nabla\Phi_h - I\|_{L^\infty(\Omega^c_{*,h})^n} \lesssim h. \tag{2.11}$$

For a finite element function $v_h \in \mathring{S}_{h,c}(\Omega^c_{*,h})$, we define $v_h^* \in L^2(\Omega)$ by

$$v_h^* = \begin{cases} v_h \circ \Phi_h^{-1} & \text{in } \Omega^c_* \\ v_h|_{\Gamma_{1,h}} \dfrac{x_n - \phi_2(x')}{\phi_1(x') - \phi_2(x')} + v_h|_{\Gamma_{2,h}} \dfrac{\phi_1(x') - x_n}{\phi_1(x') - \phi_2(x')} & \text{for } x \in \Omega_*. \end{cases} \tag{2.12}$$

By using the one-to-one correspondence between v_h^* and v_h, defined in text between (2.10) and (2.12), we can define the following deformed finite element spaces on Ω:

$$S^*_{h,c} = \begin{cases} \{v_h^* \in L^2(\Omega) : v_h \in S_{h,c}(\Omega_h)\} & \text{in Case 1} \\ \{v_h^* \in L^2(\Omega) : v_h \in S_{h,c}(\Omega^c_{*,h})\} & \text{in Case 2,} \end{cases}$$

$$\mathring{S}^*_{h,c} = \{v_h^* \in S^*_{h,c} : v_h^* = 0 \text{ on } \Gamma\}.$$

In Case 1, i.e., $\varepsilon \geq (\kappa h)^{\frac{1}{1-\alpha/2}}$, the Lagrange interpolation $I_h^* : H^1_c(\Omega) \cap C(\overline{\Omega}) \to S^*_{h,c}$ can be defined by $I_h^* v = I_h v \circ \Phi_h^{-1}$ on Ω. In Case 2, i.e., $\varepsilon \leq (\kappa h)^{\frac{1}{1-\alpha/2}}$, the Lagrange interpolation $I_h^* : H^1_c(\Omega) \cap C(\overline{\Omega}) \to S^*_{h,c}$ can be defined by

$$I_h^* v = \begin{cases} I_h v \circ \Phi_h^{-1} & \text{on } \Omega^c_*, \\ v|_{\Gamma_1} \dfrac{x_n - \phi_2(x')}{\phi_1(x') - \phi_2(x')} + v|_{\Gamma_2} \dfrac{\phi_1(x') - x_n}{\phi_1(x') - \phi_2(x')} & \text{on } \Omega_*. \end{cases}$$

By restricting I_h^* to the functions which are zero on Γ, we have $I_h^* : \mathring{H}^1_c(\Omega) \cap C(\overline{\Omega}) \to \mathring{S}^*_{h,c}$. The local error estimates of the Lagrange interpolation operator can be written as

$$\begin{aligned} \|v - I_h^* v\|_{L^\infty(\Omega_j)} &\lesssim \|v\|_{W^{k,\infty}(\Omega_j')} h_j^k && \text{for } k = 1, 2 \text{ and } j = 0, 1, \ldots, J, \\ \|v - I_h^* v\|_{W^{1,\infty}(\Omega_j)} &\lesssim \|v\|_{W^{k,\infty}(\Omega_j')} h_j^{k-1} && \text{for } k = 1, 2. \end{aligned} \tag{2.13}$$

The finite element space $\mathring{S}^*_{h,c}$ and the interpolation operator I_h^* are not available in the practical computation, but exist and can be used for analyzing the errors of the finite element solutions.

Remark 2.4. In Case 2 ($\varepsilon \le (\kappa h)^{\frac{1}{1-\alpha/2}}$) and two dimensions (i.e., $n=2$), since the function defined in (2.6) is linear on the interface $\partial\Omega_* \cap \partial\Omega_*^c$, the deformed finite element function $v_h^* \in S_h(\Omega_*^c)$ and the corresponding $v_h^* \in H^1(\Omega_*)$ are equal on the interface $\Gamma_* = \partial\Omega_{*,h}^c \cap \partial\Omega_*$ and therefore defines a function in $H^1(\Omega)$. In three dimensions, however, the function $v_h^* \in S_h(\Omega_*^c)$ and the corresponding $v_h^* \in H^1(\Omega_*)$ are not equal on the interface $\Gamma_* = \partial\Omega_*^c \cap \partial\Omega_*$ and therefore do not define a function in $H^1(\Omega)$.

2.5. The finite element method and its convergence

If $v \in L^2(\Omega) \cap H^1(\Omega_*^c) \cap H^1(\Omega_*)$ and $v = 0$ on Γ, then the solution of the perfect conductivity problem in (1.2) satisfies the following relation:

$$\int_{\Omega_*^c} \nabla u \cdot \nabla v \mathrm{d}x + \int_{\Omega_*} \nabla u \cdot \nabla v \mathrm{d}x = \int_{\Gamma_*} \partial_n u [v] \mathrm{d}\Gamma_*, \tag{2.14}$$

where $[v]$ denotes the jump of v (from Ω_* to Ω_*^c) on the interface $\Gamma_* = \partial\Omega_*^c \cap \partial\Omega_*$, and $\partial_n u$ denotes the normal derivative of u on Γ_* (with n pointing to Ω_*). If v has some kind of continuity on the interface Γ_* then the right-hand side of (2.14) would be a small remainder.

Accordingly, we consider the following finite element method for (2.14): In Case 1, $\varepsilon \ge (\kappa h)^{\frac{1}{1-\alpha/2}}$, find $u_h \in I_h\varphi + \mathring{S}_{h,c}(\Omega_h) \subset S_{h,c}(\Omega_h)$ satisfying the weak formulation

$$\int_{\Omega_h} \nabla u_h \cdot \nabla v_h \mathrm{d}x = 0 \quad \forall\, v_h \in \mathring{S}_{h,c}(\Omega_h). \tag{2.15}$$

In Case 2, $\varepsilon \le (\kappa h)^{\frac{1}{1-\alpha/2}}$, find $u_h \in I_h\varphi + \mathring{S}_{h,c}(\Omega_{*,h}^c) \subset S_{h,c}(\Omega_{*,h}^c)$ satisfying the weak formulation

$$\int_{\Omega_{*,h}^c} \nabla u_h \cdot \nabla v_h \mathrm{d}x + \int_{\Omega_*} \nabla u_h^* \cdot \nabla v_h^* \mathrm{d}x = 0 \quad \forall\, v_h \in \mathring{S}_{h,c}(\Omega_{*,h}^c), \tag{2.16}$$

where v_h^* is defined by (2.6) for any $v_h \in S_{h,c}(\Omega_{*,h}^c)$. Since a finite element function $v_h \in \mathring{S}_{h,c}(\Omega_{*,h}^c)$ matches v_h^* at the nodes on the interface Γ_*, we drop the jump term in the weak formulation of the FEM in (2.16).

For the finite element solution u_h determined by (2.16), the corresponding function u_h^* is well defined on Ω, as mentioned in the text between (2.10) and (2.12). Therefore, u_h^* can be compared with the solution u of the PDE problem. By choosing the graded mesh and finite element space defined in Section 2.2, we are able to prove optimal-order convergence of the finite element solutions uniformly with respect to ε, as shown in the following theorem.

Theorem 2.2. *For the graded mesh and finite element space defined in Section 2.2, with a pair of fixed parameters $\kappa \ge 1$ and $\alpha \in (\frac{n-1}{2}, 1+\frac{1}{n})$ that are independent of ε and h, the total number of degrees of freedom for the finite element method in* (2.16) *is $O(h^{-n})$. Moreover, under the assumptions of Theorem 2.1, the finite element solutions have the following error bounds in approximating the solution of* (1.2)*:*

$$\|u - u_h^*\|_{L^2(\Omega)} + \|\nabla(u - u_h^*)\|_{L^2(\Omega)} \le Ch,$$

where u_h^* is defined by (2.12) *and the constant C is independent of $\varepsilon \in (0, \frac{1}{2})$.*

Remark 2.5. *In Case 1, the gradient in the error bound is well defined as $u_h^* \in H^1(\Omega)$. In Case 2, the gradient in the error bound is piecewisely defined in Ω_* and Ω_*^c.*

3. Proof of Theorem 2.2

In this section, we prove Theorem 2.2 based on the results in Theorem 2.1. The proof of Theorem 2.1 is presented in the next section.

Number of degrees of freedom: Since the volume of Ω_0 is $O(1)$ and the volume of triangles/tetrahedra in Ω_0 is equivalent to h^n, it follows that the total number of triangles/tetrahedra in Ω_0 is $O(h^{-n})$.

Since $\phi_1(0) = -\phi_2(0) = \frac{\varepsilon}{2}$ and $\nabla\phi_1(0) = \nabla\phi_2(0) = 0$, it follows that $\phi_1(x) = O(\varepsilon + |x'|^2)$ and $\phi_2(x) = -O(\varepsilon + |x'|^2)$. Since Ω_j is a horizontally circular region between the two inclusions D_1 and D_2, it follows that the volume of Ω_j is

$$|\Omega_j| \sim \int_{|x'|\sim 2^{-j}} \mathrm{d}x' \int_{\phi_2(x')}^{\phi_1(x')} 1\mathrm{d}x_n \sim (\varepsilon + 2^{-2j})2^{-(n-1)j}.$$

In the case $\varepsilon \geq (\kappa h)^{\frac{1}{1-\alpha/2}}$ the integer J is defined in such a way that $2^{-J} \sim \varepsilon^{\frac{1}{2}}$, while in the case $\varepsilon \leq (\kappa h)^{\frac{1}{1-\alpha/2}}$ the integer J is defined such that $2^{-J} \sim (\kappa h)^{\frac{1}{2-\alpha}} \geq \varepsilon^{\frac{1}{2}}$. In both cases, $2^{-j} \geq \varepsilon^{\frac{1}{2}}$ for $1 \leq j \leq J$ and therefore $\varepsilon + 2^{-2j} \sim 2^{-2j}$ in Ω_j. As a result, the total number of triangles/tetrahedra in Ω_j is

$$O((\varepsilon + 2^{-2j})2^{-(n-1)j}h_j^{-n}) = O(2^{(\alpha n-n-1)j}h^{-n}).$$

In the case $\varepsilon \geq (\kappa h)^{\frac{1}{1-\alpha/2}}$ the volume of Ω_* is $O(\varepsilon^{\frac{n+1}{2}})$ and the diameter of triangles/tetrahedra in Ω_* is $O(h_*^n) = O(\varepsilon^{\frac{n\alpha}{2}}h^n)$, it follows that the total number of triangles/tetrahedra in Ω_* is

$$\varepsilon^{\frac{n+1}{2}-\frac{n\alpha}{2}}h^{-n} = O(h^{-n}) \quad \text{as } \tfrac{n+1}{2} - \tfrac{n\alpha}{2} > 0 \text{ for } \alpha \in (\tfrac{n-1}{2}, 1 + \tfrac{1}{n}).$$

In the case $\varepsilon \leq (\kappa h)^{\frac{1}{1-\alpha/2}}$ there are no degrees of freedom in Ω_*.

Overall, since $\alpha n - n - 1 < 0$ for $\alpha \in (\frac{n-1}{2}, 1 + \frac{1}{n})$ and $n \in \{2, 3\}$, the total number of degrees of freedom (number of triangles/tetrahedra) in the finite element space is equivalent to

$$h^{-n} + h^{-n} + \sum_{j=1}^{J} 2^{(\alpha n-n-1)j}h^{-n} = O(h^{-n}) \quad \text{for } \alpha \in (\tfrac{n-1}{2}, 1 + \tfrac{1}{n}).$$

Error estimates: In Case 1, by transforming u_h to u_h^*, the finite element method in (2.15) can be equivalently written as: Find $u_h^* \in I_h^*\varphi + \mathring{S}_{h,c}^*$

$$\int_\Omega A_h\nabla u_h^* \cdot \nabla v_h^*\mathrm{d}x = 0 \quad \forall\, v_h^* \in \mathring{S}_{h,c}^*, \tag{3.1}$$

where $A_h = (\nabla\Phi_h(\nabla\Phi_h)^\top \det(\nabla\Phi_h)^{-1}) \circ \Phi_h^{-1} \in L^\infty(\Omega)^{d\times d}$ satisfies the following estimate:

$$\|A_h - I\|_{L^\infty(\Omega)} \lesssim h.$$

In Case 2, by transforming u_h to u_h^*, the finite element method in (2.16) can be equivalently written as: Find $u_h^* \in I_h^*\varphi + \mathring{S}_{h,c}^*$

$$\int_{\Omega_*^c} A_h\nabla u_h^* \cdot \nabla v_h^*\mathrm{d}x + \int_{\Omega_*} \nabla u_h^* \cdot \nabla v_h^*\mathrm{d}x = 0 \quad \forall\, v_h^* \in \mathring{S}_{h,c}^*, \tag{3.2}$$

where $A_h = (\nabla\Phi_h(\nabla\Phi_h)^\top \det(\nabla\Phi_h)^{-1}) \circ \Phi_h^{-1} \in L^\infty(\Omega_*^c)^{d\times d}$ satisfies the following estimate:

$$\|A_h - I\|_{L^\infty(\Omega_*^c)} \lesssim h.$$

For the simplicity of notation, we define $A_h = I$ on Ω_* in Case 2. Then, in both Case 1 and Case 2, the FEM in (3.1) and (3.2) can be written as

$$\int_\Omega A_h \nabla u_h^* \cdot \nabla v_h^* \mathrm{d}x = 0 \quad \forall\, v_h^* \in \mathring{S}_{h,c}^*, \tag{3.3}$$

with a matrix $A_h \in L^\infty(\Omega)^{d\times d}$ satisfying the estimate $\|A_h - I\|_{L^\infty(\Omega)} \lesssim h$, where ∇u_h^* and ∇v_h^* are the piecewise gradients. The matrix A_h, the finite element space $\mathring{S}_{h,c}^*$, and the weak formulation in (3.3) are not available in the practical computation, but implicitly exist and can be used for analysis of the errors of the finite element solution given by (2.16).

Note that the finite element functions $v_h^* \in \mathring{S}_{h,c}^*$ satisfy that $v_h^* \in L^2(\Omega) \cap H^1(\Omega_*^c) \cap H^1(\Omega_*)$ and $v_h^* = 0$ on Γ. The difference between (3.3) and (2.14), with $v = v_h^*$ in (2.14), can be written as

$$\begin{aligned}
&\int_\Omega A_h \nabla (u_h^* - I_h^* u) \cdot \nabla v_h^* \mathrm{d}x \\
&= \int_\Omega (I - A_h) \nabla u \cdot \nabla v_h^* \mathrm{d}x + \int_\Omega A_h \nabla (u - I_h^* u) \cdot \nabla v_h^* \mathrm{d}x - \int_{\Gamma_*} \partial_n u [v_h^*] \mathrm{d}\Gamma_* \quad \forall\, v_h^* \in \mathring{S}_{h,c}^*.
\end{aligned} \tag{3.4}$$

Since $u_h^* - I_h^* u \in \mathring{S}_{h,c}^*$, substituting $v_h^* = u_h^* - I_h^* u$ into (3.4) leads to

$$\begin{aligned}
\|\nabla (u_h^* - I_h^* u)\|_{L^2(\Omega)}^2 &\lesssim (\|(I - A_h)\nabla u\|_{L^2(\Omega)} + \|\nabla (u - I_h^* u)\|_{L^2(\Omega)}) \|\nabla (u_h^* - I_h^* u)\|_{L^2(\Omega)} \\
&\quad + \|\partial_n u\|_{L^2(\Gamma_*)} \|[v_h^*]\|_{L^2(\Gamma_*)} \\
&\lesssim (h\|u\|_{H^1(\Omega)} + \|\nabla (u - I_h^* u)\|_{L^2(\Omega)}) \|\nabla (u_h^* - I_h^* u)\|_{L^2(\Omega)} \\
&\quad + \|\partial_n u\|_{L^2(\Gamma_*)} \|v_h^* - I_h^* v_h^*\|_{L^2(\Gamma_*)},
\end{aligned} \tag{3.5}$$

where, in the last term on the right-hand side of (3.5), we denote by v_h^* the expression

$$v_h^*|_{\Gamma_1} \frac{x_n - \phi_2(x')}{\phi_1(x') - \phi_2(x')} + v_h^*|_{\Gamma_2} \frac{\phi_1(x') - x_n}{\phi_1(x') - \phi_2(x')}.$$

Note that the area of the interface Γ_* can be estimated by

$$\begin{aligned}
|\Gamma_*| &\le \begin{cases} (\varepsilon + |\kappa h|^{\frac{2}{2-\alpha}}) & \text{in two dimensions} \\ (\varepsilon + |\kappa h|^{\frac{2}{2-\alpha}})|\kappa h|^{\frac{1}{2-\alpha}} & \text{in three dimensions} \end{cases} \\
&\le (\varepsilon + |\kappa h|^{\frac{2}{2-\alpha}})^{\frac{n}{2}} \qquad\qquad\quad \text{in } n \text{ dimensions.}
\end{aligned}$$

The last term on the right-hand side of (3.5) can be estimated as follows:

$$\|\partial_n u\|_{L^2(\Gamma_*)} \lesssim \|\partial_n u\|_{L^\infty(\Gamma_*)} |\Gamma_*|^{\frac12} \lesssim (\varepsilon + |\kappa h|^{\frac{2}{2-\alpha}})^{-\frac{n}{2}+\frac12} (\varepsilon + |\kappa h|^{\frac{2}{2-\alpha}})^{\frac{n}{4}} \lesssim (\varepsilon + |\kappa h|^{\frac{2}{2-\alpha}})^{-\frac{n}{4}+\frac12}$$

and

$$\begin{aligned}
\|v_h^* - I_h^* v_h^*\|_{L^2(\Gamma_*)} &\lesssim h_*^2 \|\nabla^2 v_h^*\|_{L^2(\Gamma_*)} \\
&\lesssim h_* \|\nabla^2 v_h^*\|_{L^\infty(\Gamma_*)} (\varepsilon + |\kappa h|^{\frac{2}{2-\alpha}})^{\frac{n}{2}} \\
&\lesssim h_* |v_h^*|_{\Gamma_1} - v_h^*|_{\Gamma_2}| (\varepsilon + |\kappa h|^{\frac{2}{2-\alpha}})^{-\frac{n}{2}} (\varepsilon + |\kappa h|^{\frac{2}{2-\alpha}})^{\frac{n}{2}} \\
&\lesssim h_* |v_h^*|_{\Gamma_1} - v_h^*|_{\Gamma_2}| \\
&\lesssim h_* \|\nabla v_h^*\|_{L^1(\Omega)} \\
&\lesssim h_* \|\nabla v_h^*\|_{L^2(\Omega)}.
\end{aligned}$$

Therefore,

$$
\begin{aligned}
\|\partial_n u\|_{L^2(\Gamma_*)}\|v_h^* - I_h^* v_h^*\|_{L^2(\Gamma_*)} &\lesssim |\kappa h|^{\frac{1-\frac{n}{2}}{2-\alpha}} h_* \|\nabla v_h^*\|_{L^2(\Omega)} \\
&\lesssim |\kappa h|^{\frac{\alpha+1-\frac{n}{2}}{2-\alpha}} h \|\nabla v_h^*\|_{L^2(\Omega)} \\
&\lesssim h\|\nabla v_h^*\|_{L^2(\Omega)} \quad (\text{since } \alpha + 1 - \tfrac{n}{2} > 0 \text{ for } n = 2, 3)
\end{aligned} \tag{3.6}
$$

Then, combining the estimates in (3.5) and (3.6), we have the following estimate for the piecewise gradient of the error:

$$
\begin{aligned}
\|\nabla(u_h^* - I_h^* u)\|^2_{L^2(\Omega)} &\lesssim h^2 + \|\nabla(u - I_h^* u)\|^2_{L^2(\Omega)} \\
&\lesssim h^2 + \|\nabla(u - I_h^* u)\|^2_{L^2(\Omega_0)} \\
&\quad + \|\nabla(u - I_h^* u)\|^2_{L^2(\Omega_*)} + \sum_{j=1}^{J} \|\nabla(u - I_h^* u)\|^2_{L^2(\Omega_j)}.
\end{aligned} \tag{3.7}
$$

Let

$$
\begin{aligned}
&\Omega_j' = \{x \in \Omega : 2^{-j-2} < |x'| \le 2^{-j+1}\}, \\
&\Omega_*' = \{x \in \Omega : |x'| \le 2^{-J}\}, \quad \Omega_0' = \{x \in \Omega : |x'| > 2^{-2}\}.
\end{aligned}
$$

Then

$$
\begin{aligned}
\|\nabla(u - I_h^* u)\|^2_{L^2(\Omega_0)} &\lesssim h^2 \|u\|^2_{H^2(\Omega_0')} \lesssim h^2, \\
\sum_{j=1}^{J} \|\nabla(u - I_h^* u)\|^2_{L^2(\Omega_j)} &\lesssim \sum_{j=1}^{J} h_j^2 \|u\|^2_{H^2(\Omega_j')} \\
&\lesssim \sum_{j=1}^{J} \int_{2^{-j-2} \le |x'| \le 2^{-j+1}} \int_{\phi_2(x')}^{\phi_1(x')} \frac{|x'|^{2\alpha} h^2}{(\varepsilon + |x'|^2)^n} \mathrm{d}x_n \mathrm{d}x' \\
&\lesssim \sum_{j=1}^{J} \int_{2^{-j-2} \le |x'| \le 2^{-j+1}} \frac{|x'|^{2\alpha} h^2}{(\varepsilon + |x'|^2)^{n-1}} \mathrm{d}x' \\
&\lesssim \sum_{j=1}^{J} \int_{2^{-j-2} \le |x'| \le 2^{-j+1}} |x'|^{2\alpha - 2n + 2} h^2 \mathrm{d}x' \\
&\lesssim \sum_{j=1}^{J} 2^{-2[\alpha - (n-1)/2]j} h^2 \\
&\lesssim h^2 \quad \text{for } \alpha \in (\tfrac{n-1}{2}, 1 + \tfrac{1}{n}).
\end{aligned}
$$

In the case $\varepsilon \ge (\kappa h)^{\frac{1}{1-\alpha/2}}$, we have

$$
\begin{aligned}
\|\nabla(u - I_h^* u)\|^2_{L^2(\Omega_*)} &\lesssim h_*^2 \|u\|^2_{H^2(\Omega_*')} \\
&\lesssim \int_{|x'| \le \varepsilon^{\frac{1}{2}}} \int_{\phi_2(x')}^{\phi_1(x')} \frac{|x'|^{2\alpha} h^2}{(\varepsilon + |x'|^2)^n} \mathrm{d}x_n \mathrm{d}x' \\
&\lesssim \int_{|x'| \le \varepsilon^{\frac{1}{2}}} \frac{|x'|^{2\alpha} h^2}{(\varepsilon + |x'|^2)^{n-1}} \mathrm{d}x'
\end{aligned}
$$

$$
\begin{aligned}
&\lesssim \int_{|x'|\leq \varepsilon^{\frac{1}{2}}} \frac{\varepsilon^\alpha h^2}{\varepsilon^{n-1}} \mathrm{d}x' \\
&\lesssim \varepsilon^{\alpha-(n-1)/2} h^2 \\
&\lesssim h^2 \quad \text{for } \alpha \in (\tfrac{n-1}{2}, 1+\tfrac{1}{n}).
\end{aligned}
$$

In the case $\varepsilon \leq (\kappa h)^{\frac{1}{1-\alpha/2}}$, the function $I_h^* u$ in Ω_* is the vertically linear interpolation of u for every fixed x'. We will prove the following result in the next section (by utilizing the notations in the proof of the regularity results).

Lemma 3.1. *Under the assumptions of Theorem 2.1, the following result holds:*

$$
\|\nabla(u - I_h^* u)\|_{L^\infty(\Omega_*)} \lesssim 1. \tag{3.8}
$$

This result plays a crucial role in the following estimate:

$$
\begin{aligned}
\|\nabla(u - I_h^* u)\|^2_{L^2(\Omega_*)} &\lesssim \int_{|x'|\leq (\kappa h)^{\frac{1}{2-\alpha}}} \int_{\phi_2(x')}^{\phi_1(x')} \mathrm{d}x_n \mathrm{d}x' \\
&\lesssim \int_{|x'|\leq (\kappa h)^{\frac{1}{2-\alpha}}} (\varepsilon + |x'|^2) \mathrm{d}x' \\
&\lesssim \varepsilon (\kappa h)^{\frac{n-1}{2-\alpha}} + (\kappa h)^{\frac{n+1}{2-\alpha}} \\
&\lesssim (\kappa h)^{\frac{n+1}{2-\alpha}} \quad \big(\text{since } \varepsilon \leq (\kappa h)^{\frac{2}{2-\alpha}}\big) \\
&\lesssim h^2 \quad \text{for } \alpha \in [\tfrac{3-n}{2}, 2) \supset (\tfrac{n-1}{2}, 1+\tfrac{1}{n}) \text{ for } n = 2, 3.
\end{aligned}
$$

By substituting the estimates of $\|\nabla(u - I_h^* u)\|^2_{L^2(\Omega_j)}$ and $\|\nabla(u - I_h^* u)\|^2_{L^2(\Omega_*)}$ into (3.7), we obtain

$$
\|\nabla(u_h^* - I_h^* u)\|^2_{L^2(\Omega)} \lesssim h^2.
$$

By using an additional triangle inequality and using the estimates of $\|\nabla(u - I_h^* u)\|^2_{L^2(\Omega_j)}$ and $\|\nabla(u - I_h^* u)\|^2_{L^2(\Omega_*)}$ again, we obtain

$$
\|\nabla(u_h^* - u)\|^2_{L^2(\Omega)} \lesssim h^2. \tag{3.9}
$$

For $x = (x', x_n)$ in the domain $R_0 = \Omega_*^c \cap \{x : |x'| \leq \frac{1}{2}\}$ the following relation holds according to the Newton–Leibniz formula:

$$
u(x', x_n) = c_1 + \int_{\phi_1(x')}^{x_n} \partial_{y_n} u(x', y_n) \mathrm{d}y_n, \tag{3.10}
$$

$$
u_h^*(x', x_n) = c_{1,h} + \int_{\phi_1(x')}^{x_n} \partial_{y_n} u_h^*(x', y_n) \mathrm{d}y_n, \tag{3.11}
$$

where c_1 and $c_{1,h}$ are the constant values of u and u_h^* on Γ_1, respectively. Since the supports of φ and $I_h^*\varphi$ do not intersect D_1, it follows that both $u_h^* - I_h^*\varphi$ and $u - \varphi$ have constant values c_1 and $c_{1,h}$ on Γ_1. Therefore, by considering the difference between the constant value on Γ_1 and the function value on Γ in the subregion Ω_0, it is easy to show that

$$
|c_1 - c_{1,h}| \lesssim \|\nabla([u_h^* - I_h^*\varphi] - [u - \varphi])\|_{L^2(\Omega_0)} \lesssim h,
$$

where the last inequality follows from (3.9). Therefore, by comparing the two expressions in (3.10) and (3.11), and then integrating the square of the result over R_0, we have

$$
\|u - u_h^*\|^2_{L^2(R_0)}
$$

$$
\begin{aligned}
&\lesssim |c_1 - c_{1,h}|^2 + \int_{|x'|\le\frac{1}{2}} \int_{\phi_2(x')}^{\phi_1(x')} |\phi_1(x') - \phi_2(x')| \int_{\phi_2(x')}^{\phi_1(x')} |\partial_{y_n}(u(x',y_n) - u_h^*(x',y_n))|^2 \mathrm{d}y_n \mathrm{d}x_n \mathrm{d}x' \\
&\lesssim |c_1 - c_{1,h}|^2 + \|\partial_{y_n}(u - u_h^*)\|^2_{L^2(R_0)} \\
&\lesssim h^2, \qquad (3.12)
\end{aligned}
$$

where the last inequality follows from (3.9). The estimate of $\|u - u_h^*\|_{L^2(\Omega\setminus R_0)}$ can be established by using the standard Poincare inequality and is therefore omitted.

This proves the first error bound in Theorem 2.2. Note that all the constants that appear in the error estimation are independent of ε. □

4. Proof of Theorem 2.1 and Lemma 3.1

The proof of Theorem 2.2 in the previous section is based on the results in Theorem 2.1 and Lemma 3.1, i.e., the pointwise asymptotic estimates for the second-order partial derivatives of the solution, and the interpolation error estimate in Ω_*. In this section we prove these results.

The asymptotic expansion of the first-order partial derivatives in the narrow region has been obtained in [24, 25, 30, 32]. We adopt the notations in [30] in the following to further derive the estimates for the second-order partial derivatives.

Proof of Theorem 2.1. In [30] it is shown that the gradient of the solution can be decomposed in the following two parts:

$$
\nabla u = (c_1 - c_2)\nabla v_1 + \nabla v_b, \qquad (4.1)
$$

where v_1 and v_b are the solution of the following two problems, respectively:

$$
\begin{cases}
\Delta v_1 = 0, & \text{in } \Omega, \\
v_1 = 1, & \text{on } \Gamma_1, \\
v_1 = 0, & \text{on } \Gamma_2 \cup \Gamma,
\end{cases}
\quad \text{and} \quad
\begin{cases}
\Delta v_b = 0, & \text{in } \Omega, \\
v_b = c_2, & \text{on } \Gamma_1 \cup \Gamma_2, \\
v_b = \varphi, & \text{on } \Gamma,
\end{cases}
\qquad (4.2)
$$

and as mentioned before the constants c_1 and c_2 are uniquely determined by the additional constraints

$$
\int_{\Gamma_i} \frac{\partial u}{\partial \nu} = 0, \qquad i = 1, 2.
$$

In [7, 30] it has been shown that

$$
|c_1 - c_2| = \frac{|B_0[\varphi]|}{\det(\nabla^2(\phi_1 - \phi_2)(0'))} \rho_n(\varepsilon)\Big(1 + O(\rho_n(\varepsilon))\Big) \qquad (4.3)
$$

where $\rho_n(\varepsilon) := \begin{cases} \sqrt{\varepsilon}, & \text{if } n = 2, \\ \frac{1}{|\log\varepsilon|}, & \text{if } n = 3, \end{cases}$ and $B_0[\varphi] = -\int_{\partial D_1^0} \frac{\partial u_0}{\partial \nu^-}$ is bounded linear functional of φ with u_0 being the solution of the touching problem

$$
\begin{cases}
\Delta u_0 = 0 & \text{in } \Omega^0 := D\setminus\overline{D_1^0 \cup D_2^0}, \\
u_0 = c_0 & \text{on } \overline{D_1^0 \cup D_2^0}, \\
\int_{\partial D_1^0} \frac{\partial u_0}{\partial \nu^-} + \int_{\partial D_2^0} \frac{\partial u_0}{\partial \nu^-} = 0 & \\
u_0 = \varphi & \text{on } \partial D.
\end{cases}
$$

Since $v_b = c_2$ on both ∂D_1 and ∂D_2, i.e., there is no difference of potential between the inclusions, it follows from [31, Theorem 1.1] that

$$
\|\nabla^2 v_b\|_{L^\infty(\Omega_{\frac{1}{2}})} \le C \quad \text{where } \Omega_{\frac{1}{2}} = \{x \in \Omega : |x'| < 1/2\}. \qquad (4.4)
$$

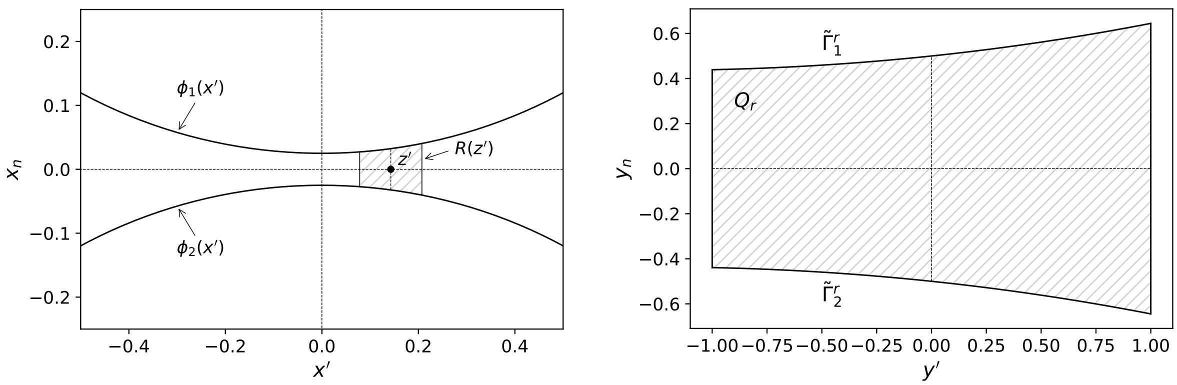

(a) Regions $R(z')$ for two different z'.

(b) Region Q_r for the region $R(z')$ on the left.

FIGURE 4.1. An illustration of the regions $R(z')$ and Q_r.

In view of this result and (4.1), it suffices to establish pointwise estimates for $\nabla^2 v_1$. To this end, we rewrite it as

$$\nabla^2 v_1 = \nabla^2 \bar{v}_1 + \nabla^2 (v_1 - \bar{v}_1),$$

where $\bar{v}_1$ is a $C^{2,\alpha}$ auxiliary function satisfying $\bar{v}_1 = 1$ on ∂D_1 and $\bar{v}_1 = 0$ on $\partial D_2 \cup \partial D$, defined by

$$\bar{v}_1(x', x_n) := \frac{x_n - \phi_2(x')}{\phi_1(x') - \phi_2(x')}. \tag{4.5}$$

Let $\delta(x') = \phi_1(x') - \phi_2(x') = \varepsilon + O(|x'|^2)$. We consider the function $w := v_1 - \bar{v}_1$, which is the solution of

$$\begin{cases} \Delta w = -\Delta \bar{v}_1 & \text{in } \Omega, \\ w = 0 & \text{on } \partial\Omega, \end{cases}$$

and estimate the second-order partial derivatives of w in the following small region (Figure 4.1):

$$R(z') := \left\{ (x', x_n) \in \Omega_{\frac{1}{2}} : \phi_2(x') < x_n < \phi_1(x'),\ |x' - z'| < \delta(z') \right\} \quad \text{for } |z'| < \tfrac{1}{2}.$$

By straightforward calculations, one can obtain the following pointwise estimates for the function $\bar{v}_1$ defined in (4.5):

$$\begin{aligned} |\nabla^2_{x'} \bar{v}_1| &\lesssim \left| \nabla_{x'} \frac{\nabla_{x'} \phi_2(x')}{\phi_1(x') - \phi_2(x')} \right| + \left| \nabla_{x'} \frac{(x_n - \phi_2(x'))(\nabla_{x'}(\phi_1(x') - \phi_2(x')))}{(\phi_1(x') - \phi_2(x'))^2} \right| \lesssim \frac{1}{\delta(x')}, \\ |\partial_{x_n} \nabla_{x'} \bar{v}_1| &= \left| \nabla_{x'} \Big(\frac{1}{\phi_1(x') - \phi_2(x')} \Big) \right| \lesssim \frac{|x'|}{\delta^2(x')} \quad \text{and} \quad \partial_{x_n x_n} \bar{v}_1 = 0 \quad \text{in } \Omega_{\frac{1}{2}}, \end{aligned} \tag{4.6}$$

and

$$|\Delta \bar{v}_1| \lesssim \frac{1}{\delta(z')},\ |\nabla \Delta \bar{v}_1| \lesssim \frac{1}{\delta^2(z')} \quad \text{in } R(z').$$

Similarly as [30, Step 2 in the proof of Proposition 1.7], we use the same translation of variables

$$\begin{cases} x' - z' = \delta(z') y', \\ x_n = \delta(z') y_n, \end{cases}$$

which transforms $R(z')$ to a cylinder Q_1 of unit size (Figure 4.1), where

$$Q_r := \left\{ (y', y_n) \in \mathbb{R}^n \mid \frac{1}{\delta(z')} \phi_2(z' + \delta(z') y') < y_n < \frac{1}{\delta(z')} \phi_1(z' + \delta(z') y'),\ |y'| < r \right\},$$

with top and bottom boundaries

$$\tilde{\Gamma}_1^r = \left\{ (y', y_n) \in \mathbb{R}^n : y_n = \tilde{\phi}_1(y') := \frac{1}{\delta(z')} \phi_1(z' + \delta(z')y') \right\},$$

and

$$\tilde{\Gamma}_2^r = \left\{ (y', y_n) \in \mathbb{R}^n : y_n = \tilde{\phi}_2(y') := \frac{1}{\delta(z')} \phi_2(z' + \delta(z')y') \right\}.$$

Since $y' = 0'$ and the height of Q_r is equal to $\frac{\phi_1(z')-\phi_2(z')}{\delta(z')} = 1$ (which is independent of ε), it follows that Q_1 is essentially a unit square in two dimensions or $B_1'(0') \times (-1/2, 1/2)$ in three dimensions as far as applications of Sobolev embedding theorems and classical L^p estimates for elliptic systems are concerned.

For simplicity, we denote

$$W(y', y_n) = w(z' + \delta(z')y', \delta(z')y_n), \quad \text{and } \bar{V}(y', y_n) = \bar{v}_1(z' + \delta(z')y', \delta(z')y_n),$$

Since $\tilde{\phi}_1$ and $\tilde{\phi}_2$ are smooth, and $W = 0$ on $\tilde{\Gamma}_2^1$, after a local smooth diffeomorphism which straightens $\tilde{\Gamma}_2^1$ to a flat boundary, similarly as [19, Proof of Theorem 9.13], we can differentiate the equation and employ the $W^{k,p}$ estimates for elliptic equations with partially vanishing boundary value to obtain the following estimates:

$$\|W\|_{W^{3,p}(Q_{1/2})} \lesssim \|\nabla W\|_{L^p(Q_{2/3})} + \|\nabla \Delta \bar{V}\|_{L^\infty(Q_1)}, \tag{4.7}$$

and

$$\|W\|_{W^{2,2}(Q_{2/3})} \lesssim \|W\|_{L^2(Q_1)} + \|\Delta \bar{V}\|_{L^\infty(Q_1)}. \tag{4.8}$$

Then, by using the Sobolev embedding $W^{2,2}(Q_{2/3}) \hookrightarrow W^{1,p}(Q_{2/3})$ and $W^{3,p}(Q_{1/2}) \hookrightarrow W^{2,\infty}(Q_{1/2})$ for some $p > n$, as well as the Poincaré inequality, from (4.7) and (4.8) we further derive the following estimate:

$$\|\nabla^2 W\|_{L^\infty(Q_{1/2})} \lesssim \|W\|_{W^{3,p}(Q_{1/2})} \lesssim \|\nabla W\|_{L^2(Q_1)} + \|\Delta \bar{V}\|_{L^\infty(Q_1)} + \|\nabla \Delta \bar{V}\|_{L^\infty(Q_1)}. \tag{4.9}$$

Rescaling the functions from $Q_{1/2}$ back to $R(z')$ and using the following relations

$$\nabla_y^2 W(y) = \delta^2(z') \nabla_x^2 w(x), \quad \nabla_y^2 \bar{V}(y) = \delta^2(z') \nabla_x^2 \bar{v}_1(x), \quad \nabla_y^3 \bar{V}(y) = \delta^3(z') \nabla_x^3 \bar{v}_1(x),$$

inequality (4.9) reduces to the following result:

$$\begin{aligned} \|\nabla^2 w\|_{L^\infty(R(z'))} \lesssim \frac{1}{\delta^2(z')} \Big(& \frac{1}{\delta^{(n-2)/2}(z')} \|\nabla w\|_{L^2(R(z'))} \\ & + \delta^2(z') \|\Delta \bar{v}_1\|_{L^\infty(R(z'))} + \delta^3(z') \|\nabla \Delta \bar{v}_1\|_{L^\infty(R(z'))} \Big). \end{aligned} \tag{4.10}$$

Then, combining (4.10) with the energy estimate $\|\nabla w\|_{L^2(R(z'))} \lesssim \delta^{n/2}(z')$, which was proved in [30, estimate (2.8)], we obtain

$$\|\nabla^2 w\|_{L^\infty(R(z'))} \lesssim \frac{1}{\delta(z')}. \tag{4.11}$$

This estimate of $w = v_1 - \bar{v}_1$ can be combined with the estimate of $\nabla^2 \bar{v}_1$ in (4.6), using the triangle inequality $|\nabla^2 v_1| \le |\nabla^2 w| + |\nabla^2 \bar{v}_1|$, to yield the following result:

$$|\nabla^2 v_1(x', x_n)| \le |\nabla^2 \bar{v}_1(x', x_n)| + |\nabla^2 w(x', x_n)| \lesssim \frac{|x'|}{\delta^2(x')} + \frac{1}{\delta(x')} \quad \text{in } \Omega_{\frac{1}{2}}. \tag{4.12}$$

In the two-dimensional case (i.e., $n = 2$), substituting (4.12) into (4.1) and using (4.3) yields the following pointwise estimate:

$$|\nabla^2 u(x', x_n)| \le |c_1 - c_2| |\nabla^2 v_1(x', x_n)| + |\nabla^2 v_b(x', x_n)|$$

$$\lesssim \frac{\sqrt{\varepsilon}|x'|}{\delta^2(x')} + \frac{\sqrt{\varepsilon}}{\delta(x')} + 1 \lesssim \frac{1}{\delta(x')} \quad \text{in } \Omega_{\frac{1}{2}}, \tag{4.13}$$

In the three-dimensional case (i.e., $n = 3$), substituting (4.12) into (4.1) and using (4.3) yields the following pointwise estimate:

$$\begin{aligned} |\nabla^2 u(x', x_n)| &\le |c_1 - c_2||\nabla^2 v_1(x', x_n)| + |\nabla^2 v_b(x', x_n)| \\ &\lesssim \frac{1}{|\log\varepsilon|}\Big(\frac{|x'|}{\delta^2(x')} + \frac{1}{\delta(x')}\Big) \quad \text{in } \Omega_{\frac{1}{2}}. \end{aligned} \tag{4.14}$$

This completes the proof of Theorem 2.1. □

Proof of Lemma 3.1. By using the relations $v_1 = \bar{v}_1 + (v_1 - \bar{v}_1)$ and $v_b = I_h^* v_b + (v_b - I_h^* v_b)$, we can rewrite (4.1) as

$$\nabla u = \nabla[(c_1 - c_2)\bar{v}_1 + I_h^* v_b] + \nabla R,$$

with $R = (c_1 - c_2)(v_1 - \bar{v}_1) + (v_b - I_h^* v_b)$. According to the definitions of v_1 and v_b in (4.2), the function $(c_1 - c_2)\bar{v}_1 + I_h^* v_b$ is linear in the x_n variable and equal to c_1 and c_2 and Γ_1 and Γ_2, respectively. This agrees with the definition of $I_h^* u$ in Ω_*, i.e.,

$$I_h^* u = (c_1 - c_2)\bar{v}_1 + I_h^* v_b \quad \text{in } \Omega_*.$$

Similarly, $I_h^* v_b$ is linear in the x_n variable and equal to c_2 on both Γ_1 and Γ_2, and therefore $I_h^* v_b \equiv c_2$ in Ω_*. Therefore,

$$\nabla u = \nabla I_h^* u + \nabla R \quad \text{in } \Omega_* \tag{4.15}$$

and $\nabla R = \nabla[(c_1 - c_2)(v_1 - \bar{v}_1) + v_b]$ in Ω_*. By substituting these relations into (4.15), we obtain

$$\begin{aligned} \|\nabla(u - I_h^* u)\|_{L^\infty(\Omega_*)} &= \|\nabla R\|_{L^\infty(\Omega_*)} \\ &= \|(c_1 - c_2)\nabla(v_1 - \bar{v}_1) + \nabla v_b\|_{L^\infty(\Omega_*)} \\ &\lesssim \|\nabla(v_1 - \bar{v}_1)\|_{L^\infty(\Omega_*)} + \|\nabla v_b\|_{L^\infty(\Omega_*)} \\ &\lesssim 1, \end{aligned} \tag{4.16}$$

where the second to last inequality is due to $|c_1 - c_2| \lesssim 1$, as shown in (4.3), and the last inequality follows from (4.4) and $\|\nabla(v_1 - \bar{v}_1)\|_{L^\infty(\Omega_*)} \lesssim 1$. The latter was proved in [30, Proposition 1.7]. □

5. Numerical experiments

In this section we present numerical experiments to support the theoretical analysis, by testing the convergence order of the method in both two- and three-dimensional spaces for both spherical and ellipsoidal close-to-touching inclusions, as well as simulating the contour and gradient of the voltage potential. The finite element meshes are generated by Gmsh [18] and visualized by Paraview [4], and the computations are performed by Firedrake [43].

In the numerical results below, the relative piecewise H^1-norm error with respect to the reference solution u_{ref} is defined by

$$\text{Relative error} = \frac{\|I_{\mathrm{ref}} u_h - u_{\mathrm{ref}}\|_{H^1}}{\|u_{\mathrm{ref}}\|_{H^1}},$$

where the reference solutions are obtained by using the proposed method with a sufficiently small mesh size, i.e., with $h = 1/256$ and $h = 1/128$ in two and three dimensions, respectively, and I_{ref} denotes the interpolation onto the reference solution's mesh. In Case 2, the H^1 norm above should be understood as the piecewise H^1 norm subject to the reference solution's mesh. We have chosen the following parameters for the graded mesh refinement: (1) $\kappa = 1$ and $\alpha = 1$

in two dimensions; (2) $\kappa = 1$ and $\alpha = 1.2$ in three dimensions. These choices are consistent with the condition $\alpha \in (\frac{n-1}{2}, 1 + \frac{1}{n})$ required in the proof of Theorem 2.2.

Example 5.1 (Circular inclusions in 2D)**.** In the first example, we consider the perfect conductivity problem in the two-dimensional rectangular domain $\Omega = (-2, 2) \times (-3, 3)$ with two circular inclusions of radius 1 centered at $(0, 1 + \epsilon/2)$ and $(0, -1 - \epsilon/2)$, respectively. The boundary potential is given by $\varphi(x, y) = y - x$.

The graded meshes in the two cases $\varepsilon = 0.1$ and $\varepsilon = 10^{-5}$, which correspond to Case 1 and Case 2 in Section 2.2, are shown in Figure 5.1. The errors of the numerical solutions given by the proposed method are presented in Figure 5.2 for the two cases. From Figure 5.2 we see that the numerical solutions in both Case 1 and Case 2 have first-order convergence in the H^1 norm, with errors almost independent of ε. This is consistent with the theoretical result proved in Theorem 2.2.

For comparison, we also present in Figure 5.2 the errors of the numerical solutions given by the standard FEM with a quasi-uniform triangulation of mesh size h, where the triangles near the origin are thin in the vertical direction in order to fit the geometry of the domain. It turns out that, for $\varepsilon = 10^{-5}$, the errors of the numerical solutions given by the standard FEM are much larger than the errors of the numerical solutions given by the proposed method.

The contour and gradient of the numerical solution in the case $\varepsilon = 10^{-5}$ are presented in Figure 5.3, where we can observe that $|\nabla u_h|$ is about 10^3 near the close-to-touching point based on the computation with mesh size $h = 1/256$. The relative error of the computation is below 0.4%, according to error in Figure 5.2 corresponding to the finest mesh.

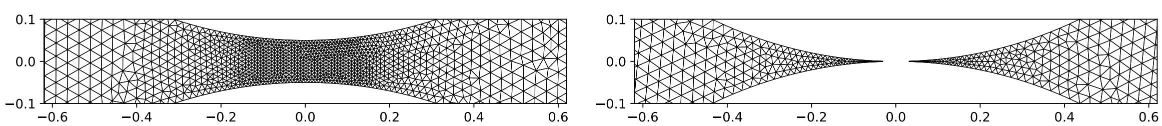

(a) $\varepsilon = 0.1$ (b) $\varepsilon = 1 \times 10^{-5}$

FIGURE 5.1. Mesh near the close-to-touching point (with $h = 1/32$).

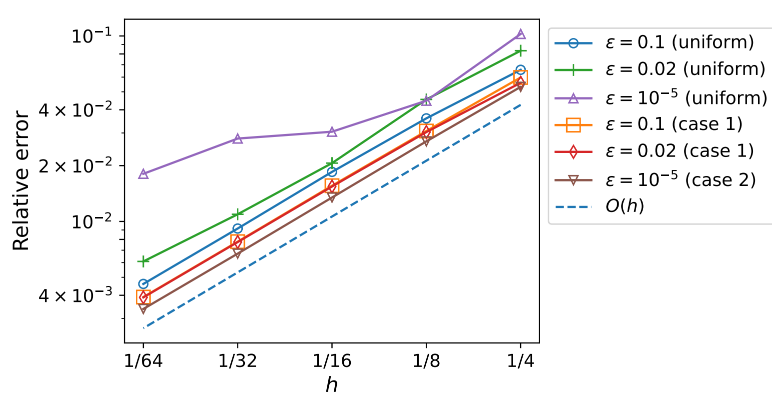

FIGURE 5.2. Relative errors in Example 5.1.

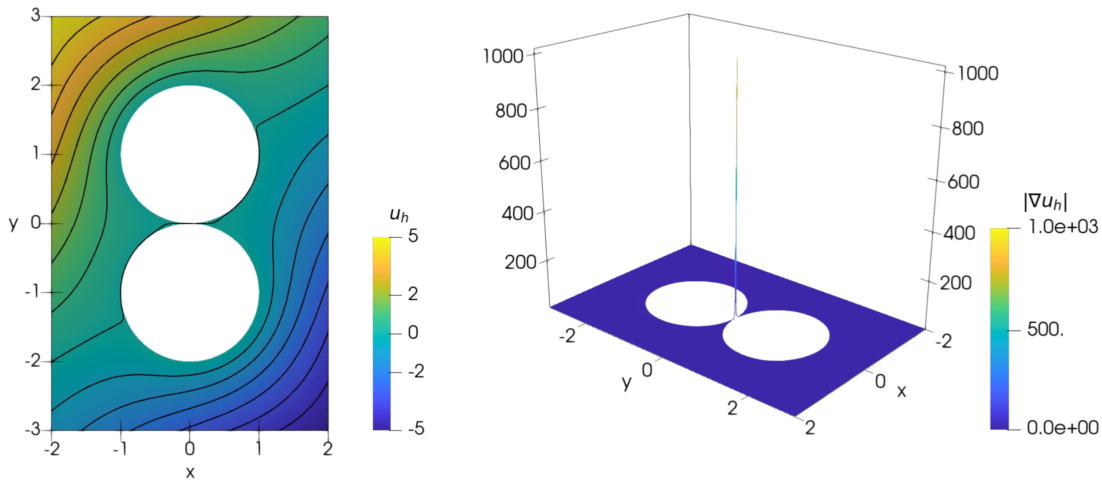

(a) Contour (b) $|\nabla u_h(x_1, x_2)|$

FIGURE 5.3. Gradient of the solution in in Example 5.1 with $\varepsilon = 10^{-5}$.

Example 5.2 (Multiple inclusions in 2D)**.** We consider nine inclusions in the domain $\Omega = [-1,1]^2$, labeled as c_{ij} and centered at $((i-2)(2a+\varepsilon), (j-2)(2a+\varepsilon))$ for $i, j \in \{1,2,3\}$. Each inclusion is a disk of radius $a = 1/4$, as shown in Figure 5.4. The minimum separation distance between these disks is ε. This example was tested in [13] with a large conductivity k inside the nine inclusions. Here we test the performance of the proposed method in the case $k = \infty$ (as considered in the current paper).

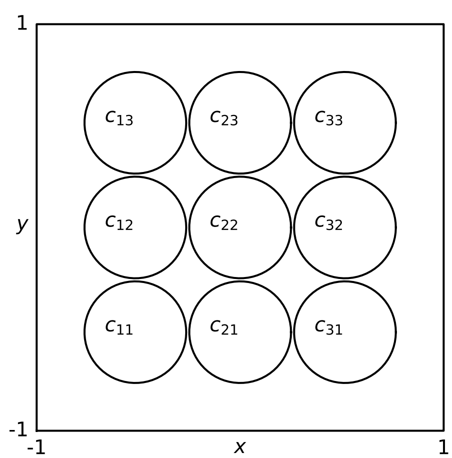

FIGURE 5.4. Domain and inclusions in Example 5.2.

We solve the perfect conductivity problem by the proposed method under the periodic boundary conditions, i.e.,

$$\begin{cases} u(x,-1) = u(x,1), & \text{for all } x \in [-1,1], \\ u(-1,y) = u(1,y) - 2, & \text{for all } y \in [-1,1]. \end{cases}$$

In Figure 5.5 we present the contour and gradient of the numerical solution in the case $\varepsilon = 10^{-5}$, where we can observe that $|\nabla u_h|$ is about 440 near the close-to-touching point. These results are consistent with the numerical simulations in [13].

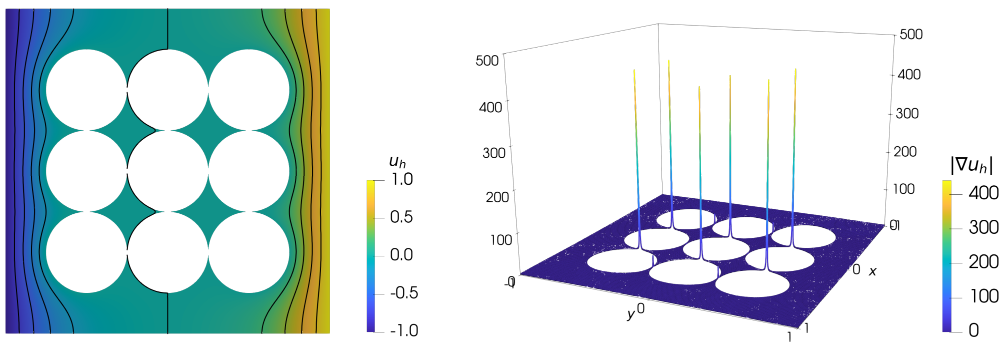

(a) Contour (b) $|\nabla u_h(x_1, x_2)|$

FIGURE 5.5. Gradient of the solution in Example 5.2, with $\varepsilon = 1 \times 10^{-5}$.

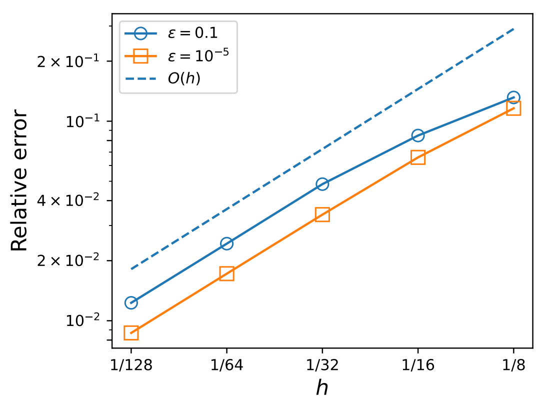

FIGURE 5.6. Relative errors in Example 5.2.

To test the convergence rates of the numerical solutions, we choose a reference solution computed from using a sufficiently small mesh size $h = 1/512$. The errors of the numerical solutions are shown in Figure 5.6 for both $\varepsilon = 0.1$ and $\varepsilon = 10^{-5}$, where first-order convergence in the H^1 norm is observed for both cases. The numerical results indicate that the proposed method and the theoretical result are also applicable to problems with multiple close-to-touching inclusions. In particular, the relative error of the numerical solution with mesh size $h = 1/128$ is below 1%.

Example 5.3 (Spherical inclusions in 3D)**.** In the second example, we consider the perfect conductivity problem in a three-dimensional domain $\Omega = [-2R, 2R] \times [-2R, 2R] \times [-3R, 3R]$ with $R = 1/2$, with two *spherical inclusions* of radius R centered at $(0, 0, R+\epsilon/2)$ and $(0, 0, -R-\epsilon/2)$, respectively. The boundary potential is given by $\varphi(x, y, z) = z - x - y$.

The graded meshes in the case $\varepsilon = 10^{-5}$ is shown in Figure 5.7, which corresponds to Case 2 in Section 2.2. The two subfigures on the right side of Figure 5.7 show a local enlargement of the mesh near the region Ω_*. The blank portion at the center of the subfigures correspond to the region Ω_*. The errors of the numerical solutions given by the proposed method are presented in Figure 5.8 for both $\varepsilon = 0.1$ and $\varepsilon = 10^{-5}$, where we see that the numerical solutions have first-order convergence in the piecewise H^1 norm with errors almost independent of ε. This is consistent with the theoretical result proved in Theorem 2.2.

The contour and gradient of the numerical solution in the case $\varepsilon = 10^{-5}$ are presented in Figure 5.9, where we can observe that $|\nabla u_h|$ is about 2×10^4 near the close-to-touching point. The relative error of the computation is below 3%, according to error in Figure 5.8 corresponding to the finest mesh.

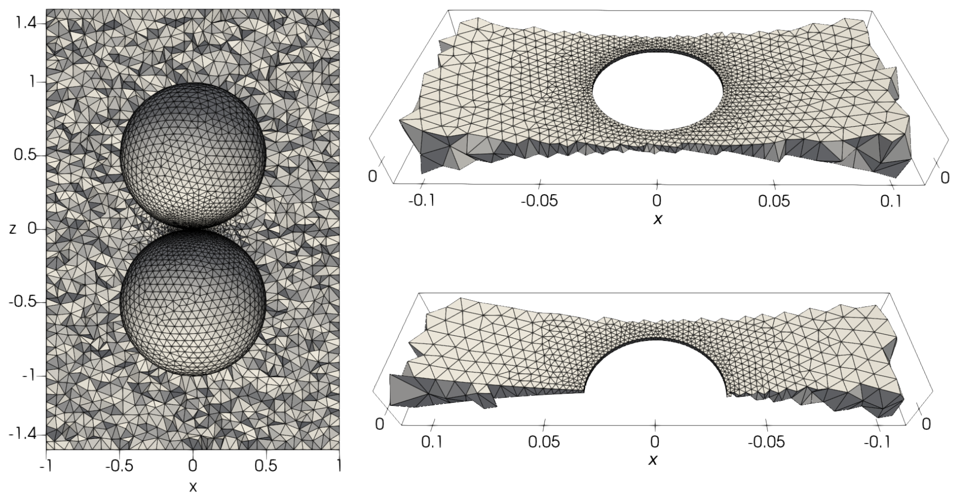

FIGURE 5.7. Mesh in Example 5.3 in the case $\varepsilon = 10^{-5}$ (with $h = 1/16$).

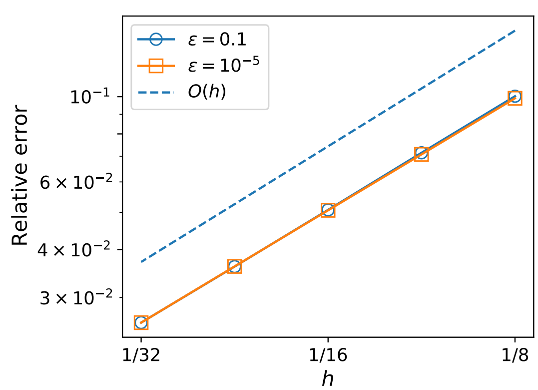

FIGURE 5.8. Relative errors in Example 5.3

Example 5.4 (Ellipsoidal inclusions in 3D)**.** In the last example, we consider the perfect conductivity problem in a three-dimensional domain $\Omega = [-2R_a, 2R_a] \times [-2R_a, 2R_a] \times [-3R_b, 3R_b]$ with two *ellipsoidal inclusions* of radii 1/2, 1/2 and $\sqrt{2}/4$ in the three directions, respectively, centered at $(0, 0, R_b + \epsilon/2)$ and $(0, 0, -R_b - \epsilon/2)$, respectively. The boundary potential is given by $\varphi(x, y, z) = z - x - y$.

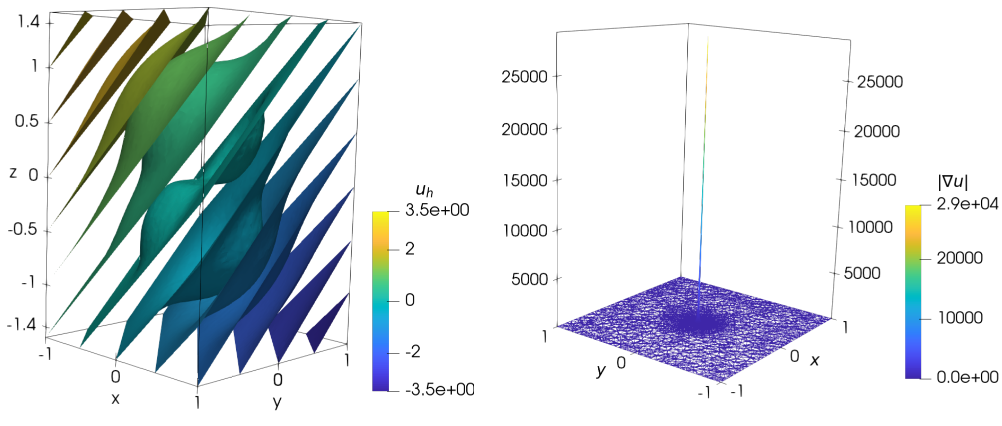

(a) Contour (b) $|\nabla u_h(x_1, x_2, 0)|$

FIGURE 5.9. Gradient of the solution in Example 5.3 with $\varepsilon = 10^{-5}$.

The graded meshes in the case $\varepsilon = 10^{-5}$ is shown in Figure 5.10. The errors of the numerical solutions given by the proposed method are presented in Figure 5.11 for both $\varepsilon = 0.1$ and $\varepsilon = 10^{-5}$, where we see that the numerical solutions have first-order convergence in the H^1 norm with errors almost independent of ε. This is consistent with the theoretical result proved in Theorem 2.2.

The contour and gradient of the numerical solution in the case $\varepsilon = 10^{-5}$ are presented in Figure 5.12, where we can observe that $|\nabla u_h|$ is about 10^4 near the close-to-touching point. The relative error of the computation is below 3%, according to error in Figure 5.11 corresponding to the finest mesh.

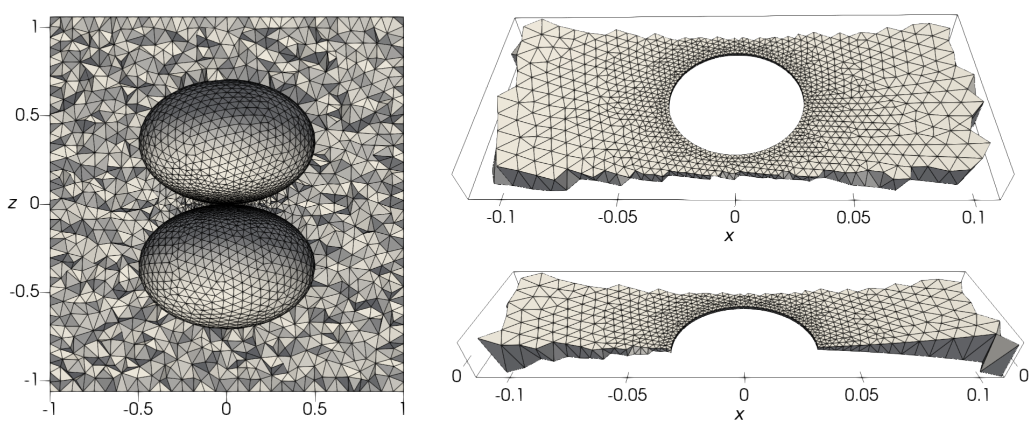

FIGURE 5.10. Mesh in Example 5.4 in the case $\varepsilon = 10^{-5}$ (with $h = 1/16$).

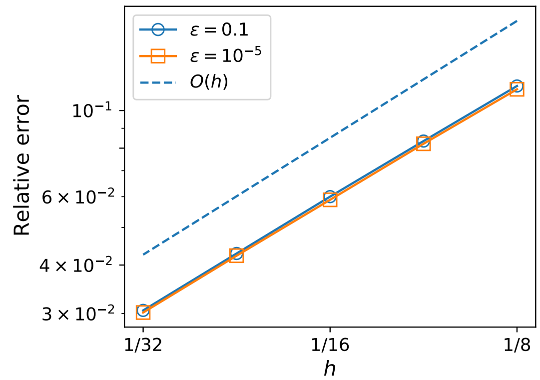

FIGURE 5.11. Relative errors in Example 5.4.

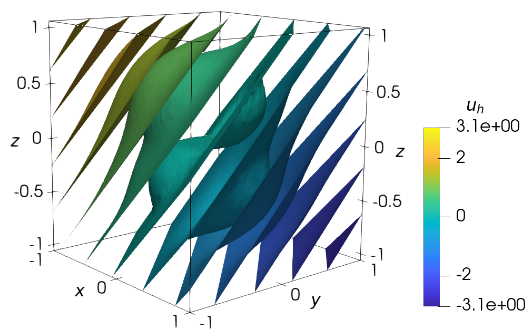

(a) Contour

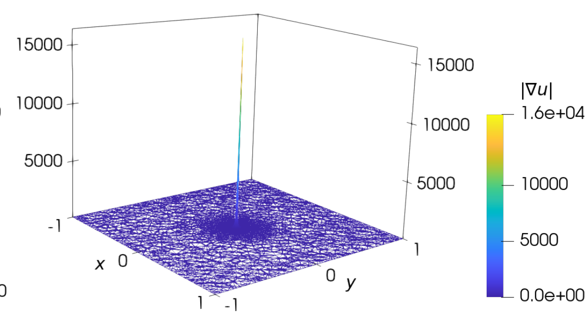

(b) $|\nabla u_h(x_1, x_2, 0)|$

FIGURE 5.12. Gradient of the solution in Example 5.4 with $\varepsilon = 10^{-5}$.

Example 5.5. In the last example, we present the total number of triangles/tetrahedra in the triangulations of Examples 5.1–5.4 in Figure 5.13, which clearly shows that the number of triangles/tetrahedra is proposal to $O(h^{-n})$ independent of ε. This is consistent with our estimate of the total number of degrees of freedom at the beginning of Section 3.

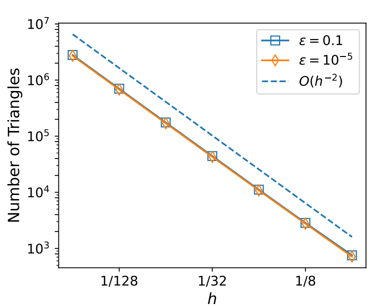

(a) Example 5.1

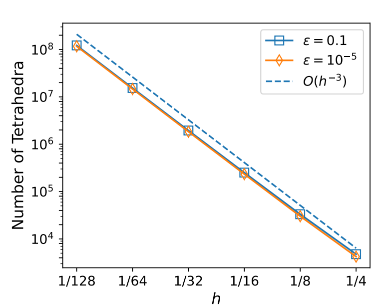

(b) Example 5.3

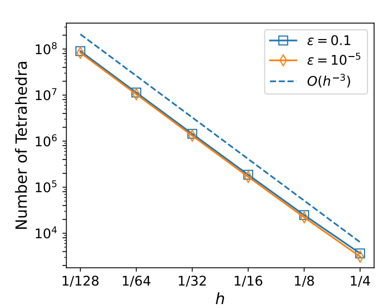

(c) Example 5.4

FIGURE 5.13. Total number of triangles/tetrahedra in Examples 5.1–5.4.

6. Conclusion

We have established new asymptotic estimates for the second-order partial derivatives of the solution to the perfect conductivity problem in a bounded smooth domain with two possibly close-to-touching convex smooth inclusions. We have used the asymptotic estimates to design a class of graded mesh and finite element spaces tailored to the asymptotic behaviour of the solution. In our construction, the mesh is refined towards the asymptotic singularity on the segment

$$L_\varepsilon = \big\{x \in \mathbb{R}^n : |x'| = 0,\ |x_n| \le \frac{\varepsilon}{2}\big\},$$

using a local mesh size $h_j \sim |x'|^\alpha h$ in Ω_j, with a parameter $\alpha \in (\frac{n-1}{2}, 1+\frac{1}{n})$ representing the rate of mesh refinement. This is different from the classical graded mesh towards a re-entrant corner x_0 with local mesh size $h_j \sim |x-x_0|^\gamma h$ and parameter $\gamma \in (1-\pi/\omega, 1)$, where ω denotes the interior angle at the re-entrant corner x_0. The difference between the 2D and 3D cases in the meshes generation lies in the range of the parameter α which characterizes the rate of mesh refinement. The range $\alpha \in (\frac{n-1}{2}, 1+\frac{1}{n})$ is different for $n = 2$ and $n = 3$ due to the different asymptotic estimates in Theorem 2.1 for the 2D and 3D cases.

In practice, graded mesh generators often use a density function to indicate the approximated size of elements locally. For the analysis we have used dyadically decomposed subregions Ω_j and local mesh size $h_j \sim |x'|^\alpha h$ in each subregion Ω_j. This follows the tradition of notations in [10, 29, 34, 44] for local error analysis based on dyadic decompositions and local regularity estimates. Alternatively, one can choose the local mesh $h(x)$ to satisfy $h(x) = O(h|x'|^\alpha)$ and then change discrete summations into integrals.

Rigorous error estimates have been established for the finite element solutions with first-order convergence in the H^1 norm uniform with respect to the distance $\varepsilon = \mathrm{dist}(D_1, D_2)$ between the inclusions. Both the computational cost and convergence rate are independent of $\varepsilon = \mathrm{dist}(D_1, D_2)$ and therefore can be applied to the case with close-to-touching inclusions. Both two- and three-dimensional problems with possibly close-to-touching inclusions are covered in a unified framework. We have presented several numerical examples to illustrate the convergence of the method. In all the examples, including 2D circular inclusions, 3D spherical inclusions and 3D ellipsoidal inclusions, the numerical results agree well with the theoretical analysis. The development of higher-order approximations to the asymptotically singular solutions, as well as the extension to other related problems with possibly close-to-touching inclusions (such as the stress concentration problem in high-contrast elastic composite materials), are still challenging and remain open.

Acknowledgements

The work of B. Li was supported in part by a grant from the Research Grants Council of the Hong Kong Special Administrative Region, China (GRF Project No. PolyU15300519). The work of H. Li was partially supported by NSF of China (No. 11971061). The work of Z. Yang was supported in part by an internal grant of The Hong Kong Polytechnic University (Project ID: P0036728, Work Programme: W18K).

References

[1] H. Ammari, E. Bonnetier, F. Triki, and M. Vogelius: Elliptic estimates in composite media with smooth inclusions: an integral equation approach. *Ann. Sci. Éc. Norm. Supér.* 48 (2015), pp. 453–495.

[2] H. Ammari, H. Kang, and M. Lim: Gradient estimates for solutions to the conductivity problem. *Math. Ann.* 332 (2005), pp. 277–286.

[3] H. Ammari, H. Kang, H. Lee, J. Lee and H. Zribi: Optimal estimates for the electric field in two dimensions. *J. Math. Pures Appl.* 88 (2007), pp. 307–324.

[4] U. Ayachit: *The ParaView Guide: A Parallel Visualization Application*. Kitware, NY, United States, 2015.

[5] I. Babuška: The finite element method for elliptic equations with discontinuous coefficients. *Computing*, 5 (1970), pp. 207–213.

[6] I. Babuška, B. Andersson, P. Smith, and K. Levin: Damage analysis of fiber composites. I. Statistical analysis on fiber scale. *Comput. Methods Appl. Mech. Engrg.* 172 (1999), pp. 27–77.

[7] E. Bao, Y. Y. Li, and B. Yin: Gradient estimates for the perfect conductivity problem. *Arch. Ration. Mech. Anal.* 193 (2009), pp. 195–226.

[8] E. Bonnetier and F. Triki: On the spectrum of the Poincaré variational problem for two close-to-touching inclusions in 2D. *Arch. Ration. Mech. Anal.* 209 (2013), pp. 541–567.

[9] E. Bonnetier and M. Vogelius: An elliptic regularity result for a composite medium with “touching” fibers of circular cross-section. *SIAM J. Math. Anal.* 31 (2000), pp. 651–677.

[10] P. Chatzipantelidis, R. D. Lazarov, V. Thomée, and L. B. Wahlbin: Parabolic finite element equations in nonconvex polygonal domains. *BIT Numer. Math.* 46 (2006), pp. S113–S143.

[11] Z. Chen and J. Zou: Finite element methods and their convergence for elliptic and parabolic interface problems. *Numer. Math*, 79 (1998), pp. 175–202.

[12] H. W. Cheng and L. Greengard: On the numerical evaluation of electrostatic fields in dense random dispersions of cylinders. *J. Comput. Phys.* 136 (1997), pp. 629–639.

[13] H. W. Cheng and L. Greengard: A method of images for the evaluation of electrostatic fields in systems of closely spaced conducting cylinders. *SIAM J. Appl. Math.* 58 (1998), pp. 122–141.

[14] D. G. Crowdy, S. Tanveer, and T. Delillo: Hybrid basis scheme for computing electrostatic fields exterior to close-to-touching discs. *IMA J. Numer. Anal.* 36 (2016), pp. 743–769.

[15] H. J. Dong: Gradient estimates for parabolic and elliptic systems from linear laminates. *Arch. Ration. Mech. Anal.* 205 (2012), pp. 119–149.

[16] H. J. Dong and H. G. Li: Optimal estimates for the conductivity problem by Green’s function method. *Arch. Ration. Mech. Anal.* 231 (2019), pp. 1427–1453.

[17] H.J. Dong, Y.Y. Li, Z.L. Yang, Optimal gradient estimates of solutions to the insulated conductivity problem in dimension greater than two, (2021), arXiv:2110.11313v1. to appear in JEMS.

[18] C. Geuzaine and J. F. Remacle: Gmsh: A 3-D finite element mesh generator with built-in pre- and post-processing facilities. *International Journal for Numerical Methods in Engineering* 79 (2009), pp. 1309–1331.

[19] D. Gilbarg and N. S. Trudinger: *Elliptic Partial Differential Equations of Second Order*, 2nd Edition, Classics Math., Springer, Berlin, 2001.

[20] L. Greengard and M. Moura: On the numerical evaluation of electrostatic fields in composite materials. *Acta Numerica* 3 (1994), pp. 379–410.

[21] J. Helsing: An integral equation method for electrostatics of anisotropic composites. *Proc. Roy. Soc. A* 450 (1995), pp. 343–350.

[22] J. Helsing: Thin bridges in isotropic electrostatics. *J. Comput. Phys.* 127 (1996), pp. 142–151.

[23] J. Huang and J. Zou: A mortar element method for elliptic problems with discontinuous coefficients. *IMA J. Numer. Anal*, 22(4):549–576, 2002.

[24] H. Kang, M. Lim, K. Yun: Asymptotics and computation of the solution to the conductivity equation in the presence of adjacent inclusions with extreme conductivities. *J. Math. Pures Appl.* 99 (2013), pp. 234–249.

[25] H. Kang, M. Lim, and K. Yun: Characterization of the electric field concentration between two adjacent spherical perfect conductors. *SIAM J. Appl. Math.* 74 (2014), pp. 125–146.

[26] J. Keller: Conductivity of a medium containing a dense array of perfectly conducting spheres or cylinders or nonconducting cylinders. *J. Appl. Phys.* 34 (1963), pp. 991–993.

[27] Y. Kim: Gradient estimates for elliptic equations with measurable nonlinearities. *J. Math. Pures Appl.* 114 (2018), pp. 118–145.

[28] M. Lenoir: Optimal isoparametric finite elements and error estimates for domains involving curved boundaries. *SIAM J Numer. Anal.* 23 (1986), pp. 562–580.

[29] B. Li: Maximum-norm stability of the finite element method for the Neumann problem in nonconvex polygons with locally refined mesh. *Math. Comp.* 91 (2023), pp. 1533–1585.

[30] H. G. Li: Asymptotics for the electric field concentration in the perfect conductivity problem. *SIAM J. Math. Anal.* 52 (2020), pp. 3350–3375.

[31] H. G. Li, Y. Y. Li, E. S. Bao, and B. Yin: Derivative estimates of solutions of elliptic systems in narrow regions. *Q. Appl. Math.* 72 (2014), pp. 589–596.
[32] H. G. Li, Y. Y. Li, and Z. L. Yang: Asymptotics of the gradient of solutions to the perfect conductivity problem. *Multiscale Model. Simul.* 17 (2019), pp. 899–925.
[33] H. G. Li, F. Wang, L. J. Xu: Characterization of electric fields between two spherical perfect conductors with general radii in 3D. J. Differential Equations 267 (2019), no. 11, 6644–6690.
[34] H. Li. The $W^{1,p}$ stability of the Ritz projection on graded meshes. *Math. Comp.*, 86:49–74, 2017.
[35] J. Li, J. M. Melenk, B. Wohlmuth, and J. Zou: Optimal a priori estimates for higher order finite elements for elliptic interface problems. *Appl. Numer. Math*, 60 (2010), pp. 19–37.
[36] Y. Y. Li and M. Vogelius: Gradient estimates for solutions to divergence form elliptic equations with discontinuous coefficients. *Arch. Ration. Mech. Anal.* 153 (2000), pp. 91–151.
[37] Y.Y. Li, Z.L. Yang, Gradient estimates of solutions to the insulated conductivity problem in dimension greater than two, arXiv:2012.14056v1. To appear in Math. Ann.
[38] E. Lindgren, A. J. Stace, E. Polack, Y. Maday, B. Stamm, and E. Besley: An integral equation approach to calculate electrostatic interactions in many-body dielectric systems. *J. Comput. Phys.* 371 (2018), pp. 712–731.
[39] G. Milton: *The Theory of Composites.* Cambridge University Press, Cambridge, 2002.
[40] R. McPhedran: Transport properties of cylinder pairs and of the square array of cylinders. *Proc. Roy. Soc. A*, 408 (1986), pp. 31–43.
[41] R. McPhedran and G. W. Milton: Transport properties of touching cylinder pairs and of the square array of touching cylinders. *Proc. Roy. Soc. A* 411 (1987), pp. 313–326.
[42] R. McPhedran, L. Poladian, and G. W. Milton: Asymptotic studies of closely spaced, highly conducting cylinders. *Proc. Roy. Soc. A* 415 (1988), pp. 185–196.
[43] F. Rathgeber, D. A. Ham, L. Mitchell, M. Lange, F. Luporini, A. T. T. Mcrae, G.-T. Bercea, G. R. Markall, and P. H. J. Kelly: Firedrake: Automating the finite element method by composing abstractions. *ACM Trans. Math. Softw.*, 43 (2017), pp. 1–27.
[44] A. H. Schatz and L. B. Wahlbin: Maximum norm estimates in the finite element method on plane polygonal domains, Part 2, Refinements. *Math. Comp.* 33 (1979), pp. 465–492.
[45] R. K. Sinha and B. Deka: A priori error estimates in the finite element method for nonself-adjoint elliptic and parabolic interface problems. *Calcolo*, 43 (2006), pp. 253–277.
[46] R. K. Sinha and B. Deka: Finite element methods for semilinear elliptic and parabolic interface problems. *Appl. Numer. Math*, 59 (2009), pp. 1870–1883.
[47] B. Weinkove, The insulated conductivity problem, effective gradient estimates and the maximum principle, (2021), arXiv:2103.14143. To appear in Math. Ann.

Buyang Li: Department of Applied Mathematics, The Hong Kong Polytechnic University, Hung Hom, Hong Kong. *E-mail address*: buyang.li@polyu.edu.hk

Haigang Li: School of Mathematical Sciences, Beijing Normal University, Laboratory of Mathematics and Complex Systems, Ministry of Education, Beijing 100875, People's Republic of China. *E-mail address*: hgli@bnu.edu.cn

Zongze Yang: Department of Applied Mathematics, The Hong Kong Polytechnic University, Hung Hom, Hong Kong. *E-mail address*: zongze.yang@polyu.edu.hk